Distribution and export of particulate organic carbon in East Antarctic coastal polynyas

Lavenia Ratnarajah[1,2*], Viena Puigcorbé[3*], Sebastien Moreau[4,5,6], Montserrat Roca-Martí[7,8], Julie Janssens[6], Matthew Corkill[6], Luis Duprat[5,6], Cristina Genovese[5,6], Jan Lieser[6,9], Pere Masqué[3,10], Delphine Lannuzel[6]

1. Antarctic Climate and Ecosystems Cooperative Research Centre, University of Tasmania, Hobart, Tasmania, Australia
2. Department of Earth, Ocean and Ecological Sciences, School of Environmental Sciences, University of Liverpool, UK
3. Centre for Marine Ecosystems Research, School of Science, Edith Cowan University, Joondalup, WA, Australia
4. Norwegian Polar Institute, Fram Centre, PO Box 6606 Langnes, NO-9296, Tromsø, Norway
5. Australian Research Council Antarctic Gateway Partnership, University of Tasmania, Hobart, Tas, Australia
6. Institute for Marine and Antarctic Studies, University of Tasmania, Hobart, Tas, Australia
7. Department of Oceanography, Dalhousie University, Halifax, Nova Scotia, Canada
8. Department of Marine Chemistry and Geochemistry, Woods Hole Oceanographic Institution, Woods Hole, Massachusetts, USA
9. Bureau of Meteorology, Hobart, Tasmania, Australia.
10. International Atomic Energy Agency, Principality of Monaco, Monaco

* Co-lead authors

Corresponding authors:

L.Ratnarajah@liverpool.ac.uk; Viena.Puigcorbe@outlook.com

Keywords

Particulate organic carbon, POC export, ^{234}Th, Polynya, Southern Ocean, East Antarctica

Key points

1. Elevated primary production leads to enhanced vertical concentration and export of particulate organic carbon (POC) in coastal polynyas in austral summer
2. POC inventories, export fluxes and export efficiencies vary significantly between polynyas
3. POC:Chl-a ratios within polynyas suggests that organic matter below the mixed layer consists largely of fresh phytoplankton at this time of the year

Abstract

Polynyas represent regions of enhanced primary production due to the low, or absent, sea-ice cover coupled with the proximity of nutrient sources. However, studies throughout the Southern Ocean suggest elevated primary production does not necessarily result in increased carbon export. Three coastal polynyas in East Antarctica and an off-shelf region were visited during the austral summer of 2016/2017 to examine the vertical distribution of particulate organic carbon (POC). Carbon export was also examined using thorium-234 (^{234}Th) as a proxy at two of the polynyas. Our results show that concentrations and integrated POC stocks were higher within the polynyas compared to the off-shelf sites. Within the polynyas, vertical POC concentrations were higher in the Mertz and Ninnis polynyas compared to the Dalton polynya. Similarly, higher carbon export was measured in the diatom-dominated Mertz polynya, where large particles (> 53 μm) represented a significant fraction of the particulate ^{234}Th and POC, compared to the small flagellate-dominated Dalton polynya, where almost all the particulate ^{234}Th and POC were found in the smaller size fraction (1 - 53 μm). The POC to Chlorophyll-a ratios suggests that organic matter below the mixed layer in the polynyas consisted largely of fresh phytoplankton at this time of the year. In combination with a parallel study on phytoplankton production at these sites, we find that increased primary production at these polynyas does lead to greater concentrations and export of POC and a higher POC export efficiency.

Plain language summary:

Polynyas are areas of open water surrounded by sea ice. In contrast to large areas of the Southern Ocean where phytoplankton growth is limited by iron, polynyas exhibit high phytoplankton biomass due to the proximity to major iron sources (e.g., melting ice, upwelling of deep water etc.). Near the ocean surface, the carbon fixed by phytoplankton can be transferred to the deeper ocean via physical and biological pathways. Yet, little is known about the magnitude and mechanisms that influence the transfer of particulate organic carbon (POC) from the surface ocean to depth in Antarctic polynyas. We examined the vertical distribution of POC in three coastal Antarctic polynyas and compared them to off-shelf sites north of the polynyas. In line with a parallel study on phytoplankton production, we find that increased phytoplankton production in polynyas led to increased vertical distribution of POC compared to off-shelf sites. However, POC stocks were higher for the Mertz and Ninnis polynyas compared to the Dalton polynya. Similarly, carbon export and export efficiencies were higher in the Mertz polynya compared to the Dalton polynya, which had smaller particles dominating the pool of POC.

1. Introduction

The biological carbon pump plays an important role in the removal of atmospheric carbon dioxide (Marinov et al. 2006). The photosynthetic production of particulate organic carbon (POC) by marine phytoplankton can globally transfer an estimated 10 Pg of carbon from the euphotic zone into the ocean interior each year (Falkowski et al. 1998, Passow and Carlson 2012). In large areas of the Southern Ocean, the scarcity of iron limits the efficiency of the biological carbon pump (Martin 1990, Boyd et al. 2017). However, the springtime melting of sea ice (Sedwick and Di Tullio 1997, Lannuzel et al. 2011), ice shelves (Herraiz-Borreguero et al. 2016), and icebergs (Lin et al. 2011), coupled with pelagic recycling (Boyd et al. 2017, Ratnarajah et al. 2018), and the resuspension of shelf sediments (Sedwick et al. 2008, McGillicuddy et al. 2015) represent important sources of iron in these high-latitude iron-limited systems, which fuel phytoplankton primary production.

In the Southern Ocean, near the Antarctic coast, sea ice is typically drifting with the Antarctic Coastal Current westward around the continent. Grounded icebergs and coastal promontories create barriers to this drift. Upstream of these barriers, sea ice accumulates and becomes fastened, while downstream, open water areas known as latent heat polynyas are maintained via katabatic winds and ocean currents that transport new ice offshore (Andersen 1993). These latent heat polynyas are acknowledged as 'sea-ice factories' due to the rapid sea-ice formation and export from the strong and persistent katabatic winds (Fraser et al. 2012). Owing to their low or absent sea-ice cover, and proximity to iron sources, coastal polynyas are characterized by intense phytoplankton blooms which account for up to 65% of total production on the Antarctic continental shelf (Arrigo and van Dijken 2003, Alderkamp et al. 2012, Gerringa et al. 2012). However, the timing, extent and intensity of primary production vary considerably amongst Antarctic polynyas. Satellite derived annual primary production estimates range from 18 ± 24 g C m^{-2} in the Lützow-Holm Bay polynya to 161 ± 37 g C m^{-2} in the Amundsen Sea polynya, with peak phytoplankton blooms occurring between December and February, depending on the polynya (Arrigo and van Dijken 2003, Arrigo et al. 2015, Liniger et al., 2020). The increased phytoplankton production supports a thriving food web from microbes to higher trophic level organisms (Karnovsky et al., 2007, Ducklow et al. 2015, Yager et al. 2016).

Sinking of POC (which includes biogenic detrital particles as well as autotrophic and heterotrophic organisms) from surface water to depth provides a mechanism for storing carbon in the deep ocean, however elevated primary production does not necessarily lead to increased carbon export. Studies have shown an increase in carbon flux with primary production due to passive sinking of organic particles (e.g., unconsumed phytoplankton, zooplankton fecal pellets) (Steinberg and Landry 2017), physical mixing via the mixed layer pump (Dall'Olmo et al. 2016), and active transport via zooplankton vertical migration (Turner 2015, Steinberg et al. 2017, Behrenfeld et al. 2019). In contrast, others demonstrated an inverse relationship between ocean primary production and export efficiency (export/net primary production (NPP)) of POC that was attributed to a combination of rapid microbial recycling, export of dissolved organic carbon, and grazer-mediated export (Maiti et al. 2013, Ducklow et al. 2015, Le Moigne et al. 2016, Lee et al. 2017, Henson et al. 2019) or by a long-time lag (e.g. 20-30 days, Henson et al. 2015) between the production and export of organic particles from the euphotic zone (Stange et al. 2017, Puigcorbé et al. 2017a, Laws and Maiti 2019). Models project that surface ocean warming in the Southern Ocean is the most important driver in NPP, coupled with relief from nutrient limitation (Laufkötter et al. 2015). With increasing temperatures, the phytoplankton community could shift towards smaller sized cells (Montes-Hugo et al. 2009, Deppeler and Davidson 2017, Treguer et al. 2018), but whilst export efficiency may decrease due to more organic carbon accumulation and remineralization in the upper ocean, changes in export production are unclear (Fan et al. 2020).

As evidenced above, POC is a highly dynamic carbon pool, and its variability is poorly constrained. In a parallel study to this, Moreau et al. (2019) measured high primary production within three coastal polynyas in East Antarctica (the Dalton, Mertz and Ninnis polynyas). Quantifying the links between surface production and POC distribution and export is key to evaluating the potential of these highly productive Antarctic coastal polynyas to export carbon now and in the future. In this study, we examine the vertical distribution of POC in these three coastal polynyas compared to an off-shelf region as a comparison, together with POC to chlorophyll-a (Chl-a) ratios, POC to particulate nitrogen (POC:PON, later referred to as C:N) ratios and ammonium concentrations, which were used as indicators of autotrophic and heterotrophic processes. Export fluxes of POC were also obtained using thorium-234 (^{234}Th, half-

life = 24.1 days) in the Dalton and Mertz polynyas to elucidate the key drivers behind the POC distribution in these coastal polynyas.

2. Methods

2.1 Site description

The sampling sites of this study are located in latent heat polynyas, west of the Dalton Iceberg Tongue (Dalton Polynya), west of the Mertz Glacier Tongue (Mertz Polynya) which was significantly shortened in 2010 (Giles 2017), and west of the Ninnis Ice Shelf (Ninnis Polynya) (Fig. 1). The three polynyas are located on the East Antarctic coastal shelf. The sea-ice encountered during sampling in late December-early January 2016/17 was in an advanced stage of melting following a peak phytoplankton bloom and was considered typical for this time of year. Off-shelf stations were also sampled during this study along the World Ocean Circulation Experiment (WOCE) SR3 repeat hydrographic line, between Tasmania and Antarctica. Measurements were taken south of the Polar Front, between 61.8°S and 67.9°S along the 140°E meridian.

A total of 71 CTD (conductivity-temperature-depth, SeaBird 704, SeaBird Inc., Bellevue, USA) casts were deployed within the Dalton (n = 19), Mertz (n = 24) and Ninnis (n = 14) polynyas, and in the off-shelf region (n = 14) moving away from the coastal polynyas (Fig. 1). Of these, 9 CTDs in the Dalton, 14 in the Mertz, 12 in the Ninnis, and 2 in the off-shelf region were sampled for *in situ* POC and PON measurements (yellow circles, Fig. 1). A total of 8 stations (4 in the Dalton and 4 in the Mertz polynyas) were also sampled for ^{234}Th (black circles, Fig. 1).

2.2 Depth categories

The euphotic depth was considered as the depth at which photosynthetic available radiation (PAR) falls to 0.1% of its surface incident value. There are various methods to calculate mixed layer depths. Melting sea ice would influence the salinity, and consequently the density gradient. Therefore, we used the sea surface density at 10 m as in de Boyer Montégut et al. (2004) and determined the depth of the upper mixed layer using the commonly applied threshold of 0.01 kg m^{-3} density increase relative to the sea surface density at 10 m (Thomson and Fine, 2003). To estimate ^{234}Th fluxes (see section 3.5), we use additional specific depth horizons: the equilibrium depth (Eq depth), which is the shallowest depth where ^{234}Th and ^{238}U are in equilibrium, and the

primary production zone (PPZ) which is defined as the depth where fluorescence is 10% of its maximum value in the water column.

2.3 Particulate organic matter concentration using Niskin bottles

Seawater samples were collected from Niskin bottles triggered at various depths during the CTD casts. Between 4 and 6 depths (10 – 200 m) were sampled for POC and PON based on the CTD PAR and Chl-a profiles (Moreau et al. 2019). Seawater samples were filtered (475 – 1,055 mL depending on organic matter content) onto pre-combusted (450°C for 12 h), 25 mm, quartz fiber filters (Advantec). All glassware in contact with POC samples were also pre-combusted prior to the voyage and subsequently rinsed with 2% v/v hydrochloric acid and ultra-high purity water between samples. Filters were then removed and placed into individual, sterile filter holders and wrapped in pre-combusted aluminum foil to limit light exposure. Filters were stored at −20°C until analysis (~6 months). Nine unused, pre-combusted filters were analyzed as 'filter blanks' to quantify background concentration of POC and PON on the filters.

Particulate organic carbon and nitrogen were determined using standard carbon-hydrogen-nitrogen combustion methods (Knap et al. 1994). Filters were removed from storage, punched to 15.9 mm diameter, and dried in an oven at 60°C overnight in muffled glass trays. 80 µL of 10% v/v hydrochloric acid was then added to each filter to remove any inorganic carbon. The acid-treated filters were subsequently dried in a desiccator overnight, folded and enclosed into 8 x 5 mm silver capsules (Elemental Microanalysis, UK) and analyzed at the Central Science Laboratory, University of Tasmania, using a Thermo Finnigan EA 1112 Series Flash Elemental Analyzer (estimated precision ~ 1%). The final POC and PON concentrations were calculated by subtracting the average carbon and nitrogen content measured in the filter blanks (3 ± 1 µg for carbon and 0.3 ± 0.1 µg for nitrogen), multiplying by the filter to punch area ratio and dividing the values by the volumes filtered. Particulate organic carbon and nitrogen measurements were not corrected for possible dissolved organic carbon and nitrogen adsorption on the filters.

2.4 POC and particulate beam attenuation coefficient

The determination of particulate organic carbon concentration from discrete bottle samples within a dense spatial grid is time and labor intensive. Therefore, we estimated the POC distribution along

the water column by relating the discrete POC concentration to the 660 nm wavelength measurements obtained with an *in situ* optical instrument (Wetlabs C-star serial no. 1421DR 25 cm pathlength). This method has been demonstrated to successfully examine the spatial and vertical distribution of POC in the past (e.g., Bishop 1999, Mishonov et al. 2003, Gardner et al. 2018a, b). The up cast transmissometer profile of the water column was used as it paired with the firing of the Niskin bottles for subsequent POC analysis in water samples. Upcast profiles were not affected by bottle firing (Supplementary Fig. 1). Baseline data were vertically averaged in 2 dbar (~2 m) bins. Factory calibration details are presented in Rosenberg and Rintoul (2017). The optical sensor output was delivered in percent units. The percent transmission (Tr) of light was then converted to total beam attenuation coefficients (c) using:

$$c = -(1 / r) * \ln (Tr / 100)$$

where c = beam attenuation coefficient (m^{-1}), r = beam path length (0.25 m), and Tr = beam transmission (%) (Gardner 1995). The beam attenuation coefficient represents the sum of attenuation due to particles (c_p), seawater (c_{sw}) and colored dissolved organic matter (CDOM). Scattering and absorption by CDOM is considered negligible in most open ocean waters including the Southern Ocean, so attenuation by particles (c_p) equals the total attenuation measured (c) minus the attenuation by water (c_{sw}):

$$c_p = c - c_{sw}$$

where c_{sw} was derived from measurements of c at 2000 m depth at the off-shelf sites (depths were above the nepheloid layer), where particle concentrations can be assumed to be negligible. A 5-point running median followed by a 7-point running mean was applied as a low-pass filter (Briggs et al., 2011).

The POC:c_p relationship was assessed based on sites where POC and c_p were simultaneously determined. Particulate attenuation, c_p, was linearly correlated with discrete POC concentration (with a coefficient of determination of $R^2 = 0.76$). There was no evidence of site differences between the *in situ* POC concentration and particulate attenuation ($p = 0.4$), which allowed for the

POC concentrations to be pooled across all CTDs for each polynya, and the off-shelf stations (Fig. 2). c_p was transformed to POC concentration (mg m^{-3}) via a single linear equation:

$$POC = 17.3 + 383.6c_p$$

2.5 Total ^{234}Th and ^{238}U activities in seawater

Seawater samples (4 L each) were collected along the water column (between 6 and 16 depths down to 230 to 800 m). After collection, samples were acidified to pH < 2 with nitric acid and spiked with a known amount of ^{230}Th and were processed using the manganese oxide co-precipitation technique (Benitez-Nelson et al. 2001, Clevenger et al. 2021). A gas flow low-level background beta counter was used on board to conduct the first counting (counting statistics < 3%) (RISØ, Denmark). Samples were recounted 6 months later to determine background activities. After the second counting, samples were processed following the method described in Puigcorbé et al. (2017a) to determine the potential losses of thorium during sample processing. ^{230}Th:^{229}Th ratios were measured using ICP-MS at the Alfred Wegener Institute (Germany) with an average recovery of 91 ± 9% (n = 107). ^{238}U activities (in dpm L^{-1}) were determined from salinity data using the relationship from Owens et al. (2011). Calibration for the efficiency of the detectors was carried out using ^{238}U standards and deep-water samples (2,000 – 2,900 m) were used to confirm the calibration.

2.6 Particulate ^{234}Th and POC using *in situ* pumps

Size-fractionated particles for the measurement of ^{234}Th and POC were collected using *in situ* pumps (ISP; McLane) in a total of 8 casts. Depending on the water column depth, one or two ISP were deployed at 100 – 160 m (hereafter shallow ISP) and 300 m (hereafter deep ISP). The pumping time varied between 1.5 to 2 h, allowing a total filtration volume of 250 – 420 L. The ISP were equipped with 142 mm diameter filter holders containing two filter types, a Nitex screen (53 µm) followed by a quartz filter (QMA, Millipore, 1 µm), thus allowing for particle size fractionation: 1 – 53 µm and > 53 µm. All filters were acid cleaned and QMAs were combusted prior to sampling.

Particulate material collected on the Nitex screens (> 53 µm) was rinsed using filtered seawater (<

0.2 μm), collected in an acid-cleaned plastic beaker and stirred to homogenize the sample. A volumetric fraction of the rinsed solution, representing 30 – 80% of the total volume, was filtered onto a pre-combusted 25 mm QMA filter for ^{234}Th and POC analyses. For ^{234}Th and POC analyses in QMAs (1 – 53 μm), a 25 mm punch was used to subsample 3 replicates from each filter. All filters were then dried overnight at 50 °C, counted for ^{234}Th at sea and recounted for background activities 6 months later, as was done for the seawater samples. After the background counting, samples were treated to analyze POC by adding hydrochloric acid to remove inorganic carbon and then measured by high temperature combustion using a Costech Elemental Analyzer. POC concentrations were calculated by subtracting the average carbon measured in dipped filter blanks before dividing by the filtered volume. Blanks for POC (5.3 ± 0.6 μg/filter, n = 3) were obtained from dipped filters and represented, on average, 1.8% ± 1.0% of the total amount measured in the samples from both size fractions (n = 56). POC and ^{234}Th measurements in triplicate QMA punches showed a relative standard deviation of 4.1 ± 2.5% and 7.6 ± 3.5%, respectively.

2.7 Ammonium in seawater

Samples from each CTD were collected to determine the concentration of ammonium in seawater using a Seal AA3 HR Auto Analyzer based on the method by Kérouel and Aminot (1997). This method is based on the reaction of ammonium with ortho-phthaldialdehyde and sulfite at a pH of 9.0 – 9.5 producing an intensely fluorescent product; with an excitation at 370 nm, and emission at 460 nm. Interferences from amino acids present in the sample are eliminated by the specific combination of the working reagent. Salt effects are eliminated by keeping the Borax buffer at pH 9.0 – 9.5. Analysis was conducted at CSIRO, Hobart. The nominal method detection limit is 0.02 μmol L^{-1}. Method uncertainty at 1.0 μmol L^{-1} is 0.066 μmol L^{-1}. Due to the unbalanced dataset along the vertical profiles, we used the nearest neighbor interpolation between data points for every 1 dbar interval, then averaged across all stations at every 5 dbar intervals to obtain the mean ammonium profile in the top 500 m.

2.8 Statistical analysis

A two-way ANOVA with interaction effect was used to determine if there was a significant difference in the relationship between POC and particulate beam attenuation coefficient by site (i.e., Dalton, Mertz, Ninnis, off-shelf). There was no evidence of site differences, thus we fit a

linear model and obtained a common line that fits all sites (Fig. 2). One-way ANOVA (Type I) was used to determine if POC concentration varied by site. A Type II ANOVA for unbalanced data was used to determine if there was a significant difference in ammonium concentration by site and C:N ratio by site and depth. Tukey HSD post hoc test was then conducted to examine the significance of differences between sites and depths and between the different depth horizons used to calculate the ^{234}Th export flux. All analyses were performed using R (R Core Team 2014).

3. Results

3.1 Euphotic and mixed layer depths

The average (± standard deviation) euphotic depths were found to be at 95 ± 56 m, 40 ± 9 m, 41 ± 6 m and 113 ± 45 m for the Dalton, Mertz and Ninnis polynyas, and the off-shelf region, respectively (Table 1). The mixed layer depths were consistently found to be shallower than the euphotic depths at 43 ± 43 m, 13 ± 1 m, 13 ± 2 m and 20 ± 7 m for the Dalton, Mertz and Ninnis polynyas, and the off-shelf region, respectively (Table 1). Three sites in the southeast of the Dalton polynya had very deep mixed layer depths between 100 and 154 m. Excluding these sites, the average mixed layer depth would be 25 ± 12 m in the Dalton polynya.

3.2 POC profiles

POC concentrations decreased with depth in the Dalton polynya and at the off-shelf stations, while in the Mertz and Ninnis polynyas, POC increased and peaked at ~30 m depth prior to decreasing with depth (Figs. 3, 4). Overall, the mean extrapolated POC profiles (black line) mostly tracked the station profiles (grey lines) but some degree of variability was observed (Fig.4). In the upper 75 m of the Dalton polynya, three stations in the southeast of the polynya had much higher surface POC concentrations.

Within the euphotic zone, the highest POC concentrations were found in the Ninnis polynya (275 ± 95 mg m^{-3}), followed by the Mertz (244 ± 71 mg m^{-3}) and Dalton (59 ± 58 mg m^{-3}) polynyas and lastly the off-shelf region (58 ± 27 mg m^{-3}; Table 1). There was a significant difference between the three polynyas ($p < 0.01$), but only the Dalton polynya was not significantly different to the off-shelf region ($p = 0.9$). A similar pattern is observed when looking at the upper 200 m, where Ninnis (138 ± 124 mg m^{-3}) > Mertz (121 ± 95 mg m^{-3}) > Dalton (60 ± 62 mg m^{-3}) > off-shelf (47

± 26 mg m^{-3}), although pairwise comparisons suggest that all 4 locations are significantly different to each other ($p < 0.01$) (Table 1). Optical spikes were evident at the bottom of some stations in the Mertz polynya (Fig. 4). As noted in the calibration report, the near bottom transmittance spikes are evident in the full 24 Hz data for some stations in the Mertz polynya (Rosenberg et al. 2017). Because these spikes are near the seafloor, they could be due to the presence of a nepheloid layer. The thickness of the nepheloid layer was calculated based on Gardner et al. (2018 a, b) which is the distance between the $c_{P\min}$ + 0.01 m^{-1} and the profile bottom depth. In the Mertz polynya nepheloid layer thickness was 159 ± 163 m and removing the nepheloid layer would remove these spikes.

Because a large fraction of the POC pool is expected to be remineralized in the upper 200 m (Henson et al. 2012), depth integrated POC (Fig. 5) is presented for the top 200 m (Fig. 5a) and for 200 – 500 m, or to the maximum depth if shallower than 500 m (Fig. 5b). Moreover, the top 200 m layer matches the depth integrated Chl-a and NPP estimates from a parallel study (Fig. 7 in Moreau et al. 2019). Depth integrated POC of the top 200 m was greatest in the Ninnis polynya (27 ± 6 g m^{-2}), followed by the Mertz polynya (23 ± 6 g m^{-2}), and were not significantly different to each other ($p = 0.1$), however they were significantly higher compared to the Dalton polynya and the off-shelf region ($p < 0.01$). The Dalton and off-shelf region were not significantly different to each other ($p = 0.3$) with slightly higher integrated POC measured in the Dalton polynya (12 ± 7 g m^{-2}) compared to the off-shelf region (9 ± 1 g m^{-2}) (Fig. 5a; Table 1). The POC stocks between 200 and 500 m across all sites were significantly lower compared to the top 200 m (Fig. 5b). Integrated POC stocks between 200 and 500 m in the Ninnis and Mertz polynyas (8 ± 1 g m^{-2} and 7 ± 3 g m^{-2}, respectively) were higher than the off-shelf region (6 ± 2 g m^{-2}). In the Dalton polynya, 13 out of the 19 sites had water column depths < 500 m (between 230 and 322 m), thus integrated POC stocks were calculated from 200 m to seafloor at these sites (4 ± 3 g m^{-2}) and were found to be lower than the other polynyas and the off-shelf sites. Omitting these 13 sites where maximum depth was less than 500 m, depth integrated POC between 200 – 500 m for the remaining 6 sites increases to that observed for the Ninnis and Mertz polynyas (7.0 ± 0.5 g m^{-2}).

3.3 POC:Chl-a

The POC:Chl-a ratios were determined based on *in situ* sampling (i.e., not optical measurements), consequently the ratios are only available for the upper 200 m. In general, the POC:Chl-a ratios were < 200 mg mg^{-1} and increased with depth (Fig. 6). POC:Chl-a ratio was > 200 mg mg^{-1} below 100 m at the off-shelf sites, and below ~150 m in the Dalton and Ninnis polynyas. The Mertz polynya was consistently < 100 mg mg^{-1} down to 200 m.

3.4 C:N ratio

The C:N ratios in the Mertz polynya and the off-shelf sites were not significantly different to each other ($p = 0.1$). However, C:N ratios for all other site pairings were significantly different from each other ($p < 0.01$; Fig. 7). The C:N ratios were generally lower than the Redfield ratio of 6.6 mol mol^{-1} in the upper 200 m (Fig. 7). In the Ninnis polynya, the C:N ratio averaged 5.7 ± 0.7 mol mol^{-1} (n = 62), while it was 4.8 ± 0.9 mol mol^{-1} (n = 73) in the Mertz polynya, 4.0 ± 0.6 mol mol^{-1} (n = 11) in the off-shelf sites, and 2.8 ± 1.7 mol mol^{-1} (n = 41) in the Dalton polynya (Fig. 7). Only the Dalton polynya showed a significant difference in C:N ratios with depth ($p < 0.01$). There were 7 instances (in green, Fig. 7) where the blanks contributed to 31 – 46 % of the total carbon measured and C:N ratios were between 1.1 and 2.6 mol mol^{-1}. There were further 3 instances (in red, Fig. 7) where the blanks contributed to 50 – 52 % to the total carbon measured and C:N ratios were between 0.8 and 0.9 mol mol^{-1}. Therefore, these measurements with a low signal to noise ratio should be taken with caution. At all other sites, C blank corrections were < 30 % of the total C measured for each sample (7.2% on average). There were no samples where the N blank correction was > 30% of the total N measured (3.3% on average). Omitting the samples where C blank corrections were > 30 %, the mean C:N ratio in the Dalton polynya increased to 4.8 ± 1.2 mol mol^{-1} and still showed a significant decrease in C:N ratios with depth ($p < 0.05$).

3.5 ^{234}Th profiles and export fluxes

The Dalton and Mertz polynyas presented markedly different ^{234}Th profiles. The Dalton polynya's ^{234}Th activity concentrations in surface waters were relatively high (≥ 2 dpm L^{-1}) and equilibrium with ^{238}U (2.4 dpm L^{-1}) was reached at depths no deeper than 100 m. In contrast, in the Mertz polynya, a clear deficit of ^{234}Th with respect to ^{238}U was present at all stations down to 70 – 125 m (Fig. 8), with ^{234}Th:^{238}U activity ratios averaging 0.66 ± 0.15 (n = 17).

^{234}Th fluxes were obtained by integrating its deficit in the upper water column with respect to ^{238}U, applying a 1D scavenging model assuming steady state conditions and considering there was no significant advection nor diffusion transport. The small ^{234}Th deficits found in the Dalton polynya led to small (<800 dpm m^{-2} d^{-1}) or even negligible ^{234}Th export fluxes (Table 2). In contrast, the ^{234}Th fluxes in the Mertz polynya were, on average, 5-fold higher than those measured in the Dalton polynya. The integration depth chosen can, in some cases, impact significantly the derived export flux. For that reason, we used four different depths horizons to calculate the ^{234}Th fluxes: i) the depth where the shallow ISP were deployed; ii) the equilibrium depth (Eq depth); iii) the primary production zone (PPZ) and iv) the depth of the euphotic zone (Zeu) (see section 2.2; Table 2). Out of the four depths horizons chosen here, only the Zeu yielded significantly different ^{234}Th fluxes ($p < 0.001$), especially in the Mertz polynya, where ^{234}Th deficits were found below the Zeu depth resulting in significantly lower ^{234}Th fluxes at this depth compared to the other deeper depth horizons. There were no significantly different results ($p > 0.5$) among the other three integration depths suggesting that PPZ, shallow ISP depth and Eq depth are a better definition of the productive layer in this study area. Moreover, since the goal is to estimate the export of POC out of the productive layer, the rationale to use the deeper horizons, where less viable phytoplankton should be expected, seems justified, henceforth we will consider the fluxes obtained at the shallow ISP depth, since those are the depths where POC:^{234}Th ratios were measured.

3.6 Particulate ^{234}Th, POC and POC:^{234}Th ratios

In the Mertz polynya, the concentrations of particulate ^{234}Th at the shallow ISP depths were >2 times higher compared to the Dalton polynya (0.321 ± 0.082 dpm L^{-1} vs 0.140 ± 0.013 dpm L^{-1}), but particulate ^{234}Th in the Dalton polynya was comparable to the concentrations measured at the deep ISP depth (300 m) in the Mertz (0.120 ± 0.013 dpm L^{-1}). The relative contribution of both particle sizes to particulate ^{234}Th was also different between polynyas. At all the stations in the Dalton polynya, almost all of the particulate ^{234}Th was measured in the small size fraction (98 ± 2%, Fig. 9). Comparatively, in the Mertz polynya the contribution of small particles to ^{234}Th was found to be smaller and more variable across stations (63 ± 19%) with a minimum contribution of 40% (EM03 at 100 m, Fig. 9). In the Mertz polynya, we observed an increase of the percentage of ^{234}Th in the small size fraction in the deep samples compared to the shallow samples (Fig. 9). The

POC distribution between the two polynyas and between the size fractions mimics that of particulate ^{234}Th, with almost the totality of POC measured in the small size fraction in the Dalton polynya, whereas in the Mertz polynya small particles still represent the larger fraction of POC albeit this fraction is smaller, with large particles representing up to 42% of the POC (Fig. 9). POC and ^{234}Th were found to significantly correlate positively in the Mertz polynya when pooling all the data available ($R^2 = 0.84$, $p = 0.00018$, $n = 14$) but also when looking at the two size fractions separately (small particles: $R^2 = 0.93$, $p = 0.0021$, $n = 7$; large particles: $R^2 = 0.88$, $p = 0.0082$, $n = 7$). In the Dalton polynya, that relationship was only significant when pooling all the dataset ($\rho^2 = 0.67$, $p = 0.029$, $n = 10$).

The POC:^{234}Th ratios, multiplied by the flux of ^{234}Th, are used to derive the POC fluxes. The shallow POC:^{234}Th ratios for small particles averaged 14 ± 9 μmol dpm^{-1} in the Dalton polynya and 9 ± 1 μmol dpm^{-1} in the Mertz polynya, whereas for large particles the averages were 35 ± 10 μmol dpm^{-1} (two stations with ratios >130 μmol dpm^{-1} not included in the average) and 6 ± 2 μmol dpm^{-1}, for the Dalton and the Mertz polynya, respectively. At 300 m, the POC:^{234}Th ratio for both size classes and polynyas was on average ~ 12 μmol dpm^{-1}. Despite some variability, the shallow POC:^{234}Th ratios in small and large particles were comparable (within a factor of 2). To derive the POC fluxes using the ^{234}Th deficits, we used the POC:^{234}Th ratios measured in the small particles in both polynyas. The rationale behind this is the fact that in the Dalton polynya ^{234}Th activities in the large particles were very low (Fig. 9) leading to unreliable large POC:^{234}Th ratios (>130 μmol dpm^{-1}) compared to global open ocean POC:^{234}Th ratios (Puigcorbé et al., 2020) and in the Mertz polynya we did not find significant differences between the POC:^{234}Th ratios measured in small and large particles ($p = 0.053$).

3.7 Ammonium in seawater

The distribution of ammonium in seawater (Fig. 10) mimicked the POC profiles observed for the polynyas (Fig. 4). Ammonium concentration in the Mertz (0.4 ± 0.5 μmol L^{-1}) and Ninnis polynyas (0.5 ± 0.6 μmol L^{-1}) were not significantly different from each other ($p = 0.9$) but were significantly higher than in the Dalton polynya (0.2 ± 0.2 μmol L^{-1}) and the off-shelf sites (0.3 ± 0.3 μmol L^{-1}) ($p < 0.01$ for both). The Dalton and the off-shelf sites were not significantly different ($p = 0.2$).

4. Discussion

4.1 Does primary production influence the vertical distribution and export of carbon?

Organic particles in the ocean originate from phytoplankton primary production. Moreau et al. (2019) recorded high Chl-a, phytoplankton biomass and net community production within these polynyas. Here we examine if the high primary production translates to substantial presence and export of POC along the water column. Within the polynyas, the highest average POC concentrations were measured in the Ninnis polynya followed by the Mertz and lastly the Dalton polynyas (Table 1, Fig. 4). In the Mertz and Ninnis polynyas, POC concentration increased with depth down to the deep Chl-a maximum depth (31 ± 9 m in the Mertz polynya and 33 ± 10 m in the Ninnis polynya; Moreau et al., 2019), and decreased thereafter (Fig. 4). In the Dalton polynya, three stations in the southeast of the polynya had much higher POC concentrations compared to the other stations sampled within the same polynya. These three stations with elevated POC in the Dalton polynya correspond to sites with higher Chl-a (Moreau et al. 2019).

Despite having similar optimal growing conditions for light and nutrients based on the maximum value of the quantum yield of photosystem II (Moreau et al. 2019), the integrated phytoplankton biomass (top 200 m) was also higher in the Mertz and Ninnis polynyas (158 - 507 mg Chl-a m^{-2} and 152 - 453 mg Chl-a m^{-2}, respectively) compared to the Dalton polynya (9 - 304 mg Chl-a m^{-2}). Similarly, net community production was significantly higher in the Mertz and Ninnis polynyas (31.2 – 106.9 g C m^{-2} and 36.0 – 68.5 g C m^{-2}, respectively) compared to the Dalton polynya (3.6 – 56.5 g C m^{-2}, Moreau et al. 2019). Integrated POC were roughly double in the Mertz and Ninnis polynyas compared to the Dalton polynya (Table 1). ^{234}Th-derived POC export was only measured in the Mertz and Dalton polynyas, and there were significant differences between both polynyas, with ^{234}Th fluxes being 5-fold higher in the Mertz compared to the Dalton polynya, leading to POC export flux in the Mertz that was, on average, ~4 times higher than in the Dalton polynya (~16 vs ~4 mmol C m^{-2} d^{-1}, respectively, Table 2). By comparing the POC export fluxes to NPP we can estimate the efficiency of the export in both polynyas. NPP estimates were inferred from nitrate drawdown in the surface layer compared to the deeper winter layer (Moreau et al. 2019), which is suggested to be a valid approach in such high latitude areas (Moreau et al. 2013, Fransson et al. 2004). The opening of the polynyas started in September/October; however, the beginning of the productive season was considered to be mid-November based on previous studies in the Dalton and Mertz polynyas (Arrigo et al. 2015, Liniger et al. 2020). Based on this assumption, we estimate

that the export efficiency in the Mertz polynya was, on average, 15%, and 2.9 times higher than in the Dalton polynya.

The off-shelf sites were not examined in Moreau et al. (2019). However, the same fluorometer was used throughout the voyage, allowing us to extrapolate the relationship presented in Moreau et al. (2019) between seawater fluorescence and Chl-a to the off-shelf sites to determine if integrated POC distribution and integrated phytoplankton biomass is different between the polynyas and the off-shelf sites. Integrated phytoplankton biomass (top 200 m) at the off-shelf sites (62 - 96 mg Chl-a m^{-2}) were lower compared to the polynyas. The CLIVAR-SR3 cruise in 2001, which followed the same transect at a similar time of the year (Nov-Dec), measured low dissolved Fe (~0.1 nM) and integrated phytoplankton biomass of 35 and 37 mg Chl-a m^{-2} at 64.9°S and 60.8°S, and 140°E (Kopczyńska et al. 2007). Nitrate and nitrite (28 – 30 μmol L^{-1}) and phosphate (1.8 – 1.9 μmol L^{-1}) concentrations measured in the upper 70 m of the water column during the CLIVAR-SR3 (Kopczyńska et al. 2007) were higher than the nitrate and phosphate measured in the Mertz and Ninnis polynyas but similar to the Dalton polynya (Moreau et al. 2019). Despite the expected inter-annual variability, in the present study Chl-a and POC concentration in the off-shelf region is markedly lower compared to the polynyas. Overall, we find that the high primary production (Moreau et al. 2019) observed in the Ninnis and Mertz polynyas, led to higher vertical concentration and export of POC compared to the Dalton polynya and off-shelf sites.

4.2 POC:Chl-a ratio as a proxy of detrital or degraded organic matter relative to living phytoplankton

The POC:Chl-a ratio can be used to describe the relative proportion of organic material (living and non-living) relative to autotrophic organisms, where POC:Chl-a < 100 mg mg^{-1} indicates living phytoplankton, POC:Chl-a < 200 mg mg^{-1} indicates phytoplankton dominated particulate organic matter, and POC:Chl-a > 200 mg mg^{-1} is considered characteristic of detrital or degraded organic matter (Liénart et al. 2016). However, it is important to note that there can be high spatio-temporal variability in the POC:Chl-a ratios due to physiological photoacclimation, variations in the community composition and phytoplankton biomass (Behrenfeld et al., 2002, 2005, 2015).

At the off-shelf sites, degraded material (POC:Chl-a > 200 mg mg^{-1}) was found below 100 m, shallower that what was observed in the polynyas. In the upper 200 m of the Mertz polynya, the POC:Chl-a ratio remained relatively constant (< 100 mg mg^{-1}) suggesting the presence of living phytoplankton through to 200 m. Based on nutrient drawdown ratios and microscope analyses of the phytoplankton communities, diatoms (*Fragilariopsis curta* and *F. cylindrus*) dominated phytoplankton biomass in the Mertz polynya (Moreau et al. 2019), and these diatoms could be exported to deeper waters. Both large and small diatom blooms are often associated with enhanced POC export (Romero and Armand 2010, Roca-Martí et al. 2017, Leblanc et al. 2018). The high ^{234}Th fluxes measured in the Mertz polynya (Fig. 8 and Table 2), where large particles contributed to a larger extent to particulate ^{234}Th and POC compared to the Dalton (Fig. 9), are in line with the higher presence of large phytoplankton in that polynya. Transfer efficiencies between 100 and 300 m (i.e., POC flux at 300 m/POC flux at 100 m) could only be calculated at three stations in the Mertz polynyas but they were, in all cases, >75%, indicating that a large proportion of the POC that reached 100 m depth ended up reaching depths of 300 m. Such high transfer efficiencies have been reported in highly productive areas of the North Atlantic and the Southern Ocean (e.g., Buesseler and Boyd, 2009) usually related to diatom blooms. Healthy diatoms have been found well below the euphotic zone (e.g. down to 4,000 m in Agusti et al. 2015) which, together with the POC:Chl-a ratio < 100 mg mg^{-1}, suggest that living diatoms may have contributed to carbon export in the Mertz polynya. Diatoms have a high silica content (Brzezinski 1985), and their blooms can lead to strong silicic acid drawdown, as was observed in the Mertz polynya (Moreau et al. 2019). Also, diatoms often produce biological glues, which may promote aggregation and hence faster sinking rates (Passow et al. 1994, Smetacek et al. 2012), with studies reporting diatom sinking rates that can exceed 700 m d^{-1} (Asper and Smith 2003, Agusti et al. 2015). Nevertheless, the lack of optical spikes (Supplementary Fig. 1) throughout the water column suggests that aggregation may not be an important factor during our narrow sampling timeframe.

The POC:Chl-a ratios in the Dalton and Ninnis polynyas gradually increased with depth and degraded material (POC:Chl-a > 200 mg mg^{-1}) was measured at depths greater than 150 m (Fig. 6). A mixed phytoplankton community of diatoms and small flagellates including *Phaeocystis antarctica* dominated in the Ninnis polynya, whilst small flagellates including *P. antarctica* dominated in the Dalton polynya (Moreau et al. 2019). In the Dalton polynya we observed that the

quasi-totality (94-100%) of the particulate ^{234}Th and POC was found in the small particles (Fig. 9), which agrees with dominance of small phytoplankton. The higher POC:Chl-a ratio in the Ninnis and Dalton polynyas coupled with the presence of a mixed phytoplankton community compared to the Mertz polynya suggest that the Ninnis and Dalton polynyas may have been at a more advanced stage of bloom at the time of sampling. Whilst DiTullio et al. (2000) demonstrated that in the Ross Sea, *P. antarctica* blooms are exported rapidly during the early spring bloom, we find that the Dalton polynya had lower POC concentrations and POC export compared to the Mertz polynya, and lower POC concentrations compared to the Ninnis polynya, where diatoms would have been the drivers of the enhanced POC concentrations.

4.3 C:N ratio as a proxy for the nutritional quality of organic matter

The C:N ratio in the natural environment is plastic and under nutrient replete conditions, values of C:N can diverge from the canonical Redfield ratio, ranging from 3 to 17 due to species specific responses, differences in growth conditions or analytical techniques (Geider and La Roche 2002, Arrigo 2005, Garcia et al. 2018). Yet, a low C:N ratio is generally attributed to N enrichment and the presence of 'fresher' material, whereas a higher C:N ratio is considered to indicate preferential remineralization of N and a more degraded pool. The C:N ratios measured here were within the reported range of phytoplankton growing under nutrient-replete conditions (Geider and La Roche 2002, Arrigo 2005, Garcia et al. 2018) but they did differ between sites. The C:N ratio in the Ninnis polynya (5.7 ± 0.7) was the closest one to the Redfield ratio (6.6), while ratios below the Redfield ratio were observed at the other sites (Mertz polynya 4.8 ± 0.9, Dalton polynya 4.8 ± 1.2 and off-shelf sites 4.0 ± 0.6; Fig. 7). The C:N ratios measured in the Dalton, Mertz and Ninnis polynyas fall within the natural variability observed in the euphotic layer of the Ross Sea (5.4 – 9.2; Fabiano et al. 1993) and the Amundsen Sea polynya (6.3 – 9.2; Kim et al. 2018), whereas the off-shelf sites are slightly below those ranges. The stoichiometry of remineralization is a function of the nutritional demand of the heterotrophic population (Turley and Mackie 1994, Sterner and Elser 2002, Burkhardt et al. 2014, Letscher and Moore 2015). In some areas of the Southern Ocean, heterotrophic bacteria have been shown to be carbon limited (Church et al. 2000, Obernosterer et al. 2015). Therefore, it is possible that heterotrophic bacteria were preferentially consuming the carbon at the off-shelf sites, leading to the lower C:N ratios, which could also be the cause of the decreasing C:N ratios with depth in the Dalton polynya.

572 **4.4 Ammonium as an indicator of heterotrophic communities**

573 The high concentration of ammonium could indicate the presence of heterotrophic communities
574 (Fig. 10). The production of ammonium by bacteria and zooplankton is an important process in
575 the marine nitrogen cycle as phytoplankton (both eukaryotes and cyanobacteria) utilize ammonium
576 before nitrate due to the reduced energy costs. However, heterotrophic bacteria are also
577 competitors with phytoplankton for ammonium (Hoch and Kirchman 1995). The concentration of
578 ammonium measured in the present study fall within the summer values measured previously in
579 the Southern Ocean (~ 0.05 – 1.03 μmol L^{-1}, Bianchi et al. 1997, Mengesha et al. 1998), around
580 the Antarctic Peninsula (0.9 – 10 μmol L^{-1}, Koike et al. 1986, Owens et al. 1991, Karl et al. 1996,
581 Garibotti et al. 2003), and in the Ross Sea (4 μmol L^{-1}, Gordon et al. 2000). The highest ammonium
582 concentrations were found in the Ninnis and the Mertz polynyas (2.2 – 2.4 μmol L^{-1}) in line with
583 the deep Chl-a and POC maxima. As expected, the lower POC in the Dalton polynya and the off-
584 shelf sites were accompanied by lower ammonium concentrations (0.9 – 1.1 μmol L^{-1}).
585
586 As ammonium is released by both the bacterial and zooplankton communities, it is not possible to
587 distinguish the influence of these heterotrophic communities on the distribution of POC. However,
588 the distribution of ammonium resembles that of POC, which indicates that grazing and/or
589 remineralization track POC, rather than being concentrated at a particular depth horizon or light
590 level. Moreau et al. (2020) recently showed that grazers consume about 90% of the phytoplankton
591 in the sea-ice zone of the Southern Ocean. The fact that the ammonium profiles mirrored the
592 vertical distribution of POC could suggest that POC may not escape the heterotrophic community
593 very effectively while sinking, leading to a low carbon export efficiency. This could be particularly
594 the case in the Dalton polynya, where the average export efficiency was found to be 5%, similar
595 to export efficiencies observed in oligotrophic areas (e.g., Puigcorbé et al. 2017b), with decreasing
596 C:N ratios with depth potentially due to preferential remineralization of C by bacteria (e.g., Church
597 et al. 2000), compared to 15% export efficiency in the Mertz polynya where we also estimated
598 high transfer efficiencies down to 300 m. The differences in planktonic community composition
599 might be the reason why we observed differences in export efficiency between the Dalton and the
600 Mertz polynya, regardless of both having ammonium profiles that resemble the POC profiles.
601
602

5. Conclusion and future work

The higher primary production within the Mertz, Ninnis and Dalton polynyas resulted in higher vertical concentrations and stocks of POC along the water column within the polynyas compared to the off-shelf sites. As shown in other studies, primary production can vary greatly between polynyas. Here, vertical concentration of POC was greater in the Mertz and Ninnis polynyas compared to the Dalton polynya, and this translated to 3 - 5 times higher carbon export observed in the Mertz compared to the Dalton. The POC:Chl-a ratios of < 200 mg mg^{-1} in the upper 150 m in the Mertz, Ninnis and Dalton polynyas suggests that organic particles consisted largely of phytoplankton whilst the C:N ratios were within the reported range for being nutrient replete. However, the concentrations and stocks of POC were found to be significantly different amongst the polynyas, suggesting that the factors controlling the distribution of POC would differ between the polynyas, thereby influencing carbon export. In the Mertz polynya, the relatively constant low POC:Chl-a ratio down to 200 m (Fig. 6) indicates that POC largely consisted of fresh material, which is in line with the high transfer efficiency observed in that polynya, while in the Ninnis, Dalton and off-shelf sites, the POC:Chl-a ratios increased with depth pointing towards an increase in degraded material. The C:N ratios measured in this study suggest a high nutritional quality of the organic matter, which would encourage the presence of heterotrophic communities. Interestingly, the ammonium profiles follow the POC profiles, suggesting that these heterotrophic communities were degrading the POC throughout the water column.

The polynya specific differences highlighted here provide an interesting framework for future work. Under future climate scenarios where phytoplankton community structure in the Mertz could switch towards smaller sized cells akin to the Dalton polynya, then our study suggests that the biologically mediated carbon export in these coastal polynyas may decrease. However, patterns of remineralization and grazing may also change depending on the response of the bacterial and zooplankton communities to temperature and resource supply (e.g., iron and dissolved organic carbon availability to phytoplankton and metabolic demand of zooplankton), both of which are highly uncertain. Therefore, quantifying the micronutrients and dissolved organic carbon content in this region coupled with the rate of bacterial remineralization of sinking particles and zooplankton community dynamics will provide better insight into carbon cycling and improve its predictability in these highly productive regions under future climate scenarios.

Acknowledgments and Data Availability

This study was supported by the Australian Government's Cooperative Research Centres through the Antarctic Climate and Ecosystem Cooperative Research Centre, the Australian Antarctic Division research projects AAS 4131 and 4291, and the Institute for Marine and Antarctic Studies, University of Tasmania. L. Ratnarajah also received support from BYONIC (ERC award number 724289). D. Lannuzel was supported by an Australian Research Council Future Fellowship (Project ID L0026677). S. Moreau and C. Genovese were supported by the Australian Research Council's Special Research Initiative for Antarctic Gateway Partnership (Project ID SR140300001). V. Puigcorbé was supported by Edith Cowan University through an Early Career Researcher Grant (G1003456) and an ECU-Collaboration Enhancement Scheme grant. M. Roca-Martí was supported by funding from the Woods Hole Oceanographic Institution's Ocean Twilight Zone study and the Ocean Frontier Institute. Thanks to Thomas Rodemann at the Central Science Laboratory, University of Tasmania, Australia for the POC analyses, to Stephen Tibben and the Marine National Facility, CSIRO, Australia for ammonium analyses, to Walter Geibert, Alfred Wegener Institute (Germany), for thorium recovery analyses, and to Tom Trull for providing critical comments on the development of this manuscript. We acknowledge the use of imagery from the NASA Worldview application (https://worldview.earthdata.nasa.gov), part of the NASA Earth Observing System Data and Information System (EOSDIS). The IAEA is grateful for the support provided to its Environment Laboratories by the Government of the Principality of Monaco. Lastly, the authors would like to thank the officers and crew of the RSV Aurora Australis for their logistical support.

Data presented in this study can be sourced from https://metadata.imas.utas.edu.au/geonetwork/srv/eng/metadata.show?uuid=02364e10-ebc0-463a-b690-2c4ed643733c.

References

Alderkamp, A., M. Mills, G. L. van Dijken, P. Laan, C. E. Thuróczy, L. J. A. Gerringa, H. J. W. De Baar, C. D. Payne, R. J. W. Visser, A. G. J. Buma and K. R. Arrigo (2012). Iron from melting glaciers fuels phytoplankton blooms in the Amundsen Sea (Southern Ocean): Phytoplankton characteristics and productivity. Deep Sea Research Part II: Topical Studies in Oceanography 71-76(15): 32-48.

Andersen, P. S. (1993). Evidence for an Antarctic winter coastal polynya. Antarctic Science 5(2): 221-226.

Agusti, S., J. I González-Gordillo, D. Vaqué, M. Estrada, M. I. Cerezo, G. Salazar, J. M. Gasol and C. M. Duarte (2015) Ubiquitous healthy diatoms in the deep sea confirm deep carbon injection by the biological pump. Nature Communications 6: 1-8

Arrigo, K. R. and G. L. van Dijken (2003). Phytoplankton dynamics within 37 Antarctic coastal polynya systems. Journal of Geophysical Research 108 (C8) (3271): 27-22 - 27-18.

Arrigo, K. R., G. L. van Dijken and A. L. Strong (2015). Environmental controls of marine primary productivity hot spots around Antarctica. Journal of Geophysical Research: Oceans 120: 5545-5565.

Arrigo, K. R (2005). Marine microorganisms and global nutrient cycles. Nature 437: 349-355

Asper, V. L. and W. O. Smith (2003). Abundance, distribution and sinking rates of aggregates in the Ross Sea, Antarctica. Deep-Sea Research I: Oceanographic Research Papers 50 (1): 131-150.

Behrenfeld, M. J., Marañón, E., Siegel, D. A., and S. B. Hooker (2002). Photoacclimation and nutrient-based model of light-saturated photosynthesis for quantifying oceanic primary production. *Mar. Ecol. Prog. Ser.* 228, 103–117.

Behrenfeld, M. J., Boss, E., Siegel, D. A., and D. M. Shea (2005). Carbon-based ocean productivity and phytoplankton physiology from space. *Glob. Biogeochem.* 19.

Behrenfeld, M. J., O'Malley, R. T., Boss, E. S., Westberry, T. K., Graff, J. R., Halsey, K. H., et al. (2015). Revaluating ocean warming impacts on global phytoplankton. *Nat. Clim. Change* 6, 323–330.

Behrenfeld, M. J., P. Gaube, A. Della Penna, R. T. O'Malley, W. J. Burt, H. Yongxiang, P. S. Bontempi, D. K. Steinberg, E. S. Boss, D. A. Siegel, C. A. Hostetler, P. D. Tortell and S. C. Doney (2019). Global satellite-observed daily vertical migrations of ocean animals. Nature 576: 257-261.

Benitez-Nelson, C. R., K. O. Buesseler, M. Rutgers van der Loeff, J. Andrews, L. Ball, G. Crossin and M. A. Charette (2001). Testing a new small-volume technique for determining ^{234}Th in seawater. Journal of Radioanalytical and Nuclear Chemistry 248: 795-799.

Bianchi, M., F. Feliatra, P. Tréguer, M. Vincendeau and J. Morvan (1997). Nitrification rates, ammonium and nitrate distribution in the upper layers of the water column and in sediments of the Indian sector of the Southern Ocean. Deep Sea Research II: Topical Studies in Oceanography 5: 1017-1032.

Bishop, J. K. B. (1999). Transmissometer measurement of POC. Deep Sea Res. I: Oceanographic Research Papers 46: 353-369.

693 Boyd, P. W., M. J. Ellwood, A. Tagliabue and B. S. Twining (2017). Biotic and abiotic retention, recycling
694 and remineralization of metals in the ocean. Nature Geoscience 10: 167-173
695 Briggs, N., Perry, M. J., Cetinić, I., Lee, C., D'Asaro, E., Gray, A. M., et al. (2011). High-resolution
696 observations of aggregate flux during a sub-polar North Atlantic spring bloom. *Deep Sea Res. Part I*58,
697 1031–1039.
698 Brzezinski, M. A. (1985). The Si:C:N ratio of marine diatoms: interspecific variability and the effect of some
699 environment variables. Journal of Phycology 21: 347-357.
700 Buesseler, K. O. and Boyd, P. W. (2009). Shedding light on processes that control particle export and flux
701 attenuation in the twilight zone of the open ocean. Limnology and Oceanography, 54(4), 1210-1232.
702 Burkhardt, B. G., K. S. Watkins-Brandt, D. Defforey, A. Payton and A. E. White (2014). Remineralization
703 of phytoplankton-derived organic matter by natural populations of heterotrophic bacteria. Marine
704 Chemistry 163: 1-9
705 Church, M. J., D. A. Hutchins, and H. W. Ducklow (2000). Limitation of bacterial growth by dissolved
706 organic matter and iron in the Southern Ocean. Applied and Environmental Microbiology 66 (2):455-466
707 Clevenger, S. J., C. R Benitez-Nelson, J. Drysdale, S. Pike, V. Puigcorbé and K. O. Buesseler (2021).
708 Review of the analysis of ^{234}Th in small volume (2-4 L) seawater samples: improvements and
709 recommendations. Journal of Radioanalytical and Nuclear Chemistry 329, 1-13.
710 Dall'Olmo, G., J. Dingle, L. Polimene, R. J. W. Brewin and H. Claustre (2016). Substantial energy input to
711 the mesopelagic ecosystem from the seasonal mixed-layer pump. Nature Geoscience 9: 820-823.
712 de Boyer Montégut, C., G. Madec, A. S. Fischer, A. Lazar and D. Iudicone (2004). Mixed layer depth over
713 the global ocean: An ecxamination of profile data and a profile-based climatology. Journal of Geophysical
714 Research 109: 1-20.
715 Deppeler, S. and A. Davidson (2017). Southern Ocean phytoplankton in a changing climate. Frontiers in
716 Marine Science 4 (40): 1-29.
717 DiTullio, G. R., J. M. Grebmeier, K. R. Arrigo, M. P. Lizotte, D. H. Robinson, A. Leventer, J. P. Barry, M.
718 L. VanWoert and R. B. Dunbar (2000). Rapid and early export of Phaeocystis antarctica bloom in the
719 Ross Sea, Antarctica. Nature 404: 595-598.
720 Ducklow H.W., S.E. Wilson, A. F. Post, S. E. Stammerjohn, M. Erickson, S.H. Lee, K. E. Lowry, R. M.
721 Sherrel and P. L. Yager (2015). Particle flux on the continental shelf in the Amundsen Sea Polynya and
722 Western Antarctic Peninsula. Elementa: Science of the Anthropocene 1-20
723 Fabiano, M., P. Povero and R. Danovaro (1993). Distribution and composition of particulate organic matter
724 in the Ross Sea (Antarctica). Polar Biol 13: 525-533.
725 Falkowski, P. G., R. T. Barber and V. Smetacek (1998). Biogeochemical Controls and Feedbacks on Ocean
726 Primary Production. Science 281(5374): 200-206.

727 Fan, G., Z. Han, W. Ma, S. Chen, F. Chai, M.R. Mazloff, J. Pan and H. Zhang (2020). Southern Ocean
728 carbon export efficiency in relation to temperature and primary productivity. Scientific Reports 10
729 (13494): 1-11.
730 Fraser, A. D., R. A. Massom, K. J. Michael, B. Galton-Fenzi and J. L. Lieser (2012). East Antarctic Landfast
731 Sea Ice Distribution and Variability, 2000-08. American Meteorological Society 25(4): 1137-1156.
732 Frasson A., M. Chierici, L. G. Anderson, R. David (2004). Transformation of carbon and oxygen in the
733 surface layer of the eastern Atlantic sector of the Southern Ocean. Deep-Sea Research II, 51: 2757-2772.
734 Garcia, N. S., J. Sexton, T. Riggins, J. Brown, M. W. Lomas and A. C. Martiny (2018). High variability in
735 cellular stoichiometry of carbon, nitrogen and phosphorus within classes of marine eukaryotic
736 phytoplankton under sufficient nutrient conditions. Frontiers in Microbiology 9 (543): 1-10.
737 Gardner, W. D, M. J. Richarson, A. V. Mishonov and P. E. Biscaye (2018a). Global comparison of benthic
738 nepheloid layers based on 52 years of T nephelometer and transmissometer measurements. Progress in
739 Oceanography 168: 100 - 111
740 Gardner, W. D, M. J. Richarson and A. V. Mishonov (2018b). Global assessment of benthic nepheloid layers
741 and linkage with upper ocean dynamics. Earth and Planetary Science Letters 482: 126 - 134
742 Gardner, W. D, S. P. Chung, M. J. Richarson, and I. D. Walsh (1995). The oceanic mixed layer pump. Deep
743 Sea Research Part II: Topical Studies in Oceanography 42: 757-775
744 Garibotti, I. A., M. Vernet, M. E. Ferrario, R. C. Smith, R. M. Ross and L. B. Quentin (2003). Phytoplankton
745 spatial distribution patterns along the western Antarctic Peninsula (Southern Ocean). Marine Ecology
746 Progress Series 261: 21-39.
747 Geider, R. J. and J. La Roche (2002). Redfield revisited: variability of C:N:P in marine microalgae and its
748 biochemical basis. European Journal of Phycology 37: 1-17.
749 Gerringa, L. J. A., A.-C. Alderkamp, P. Laan, C. E. Thuróczy, H. J. W. De Baar, M. M. Mills, G. L. van
750 Dijken, H. van Haren and K. R. Arrigo (2012). Iron from melting glaciers fuels the phytoplankton blooms
751 in Amundsen Sea (Southern Ocean): Iron biogeochemistry. Deep Sea Research II: Topical Studies in
752 Oceanography 71-76(15): 16-31.
753 Giles, A. B. (2017). The Mertz Glacier Tongue, East Antarctica. Changes in the past 100 years and its cyclic
754 nature - Past, present and future. Remote Sensing of Environment 191: 30-37.
755 Gordon, L. I., L. A. Codispoti, J. C. Jennings Jr, F. J. Millero, J. M. Morrison and C. Sweeney (2000).
756 Seasonal evolution of hydrographic properties in the Ross Sea, Antarctica, 1996–1997. Deep Sea
757 Research II: Topical Studies in Oceanography 47: 3095-3117.
758 Henson, S. A., A. Yool and R. Sanders (2015). Variability in efficiency of particulate organic carbon export:
759 A model study. Global Biogeochemical Cycles 29 (1): 33-45.

760 Henson, S., F. Le Moigne and S. Giering (2019). Drivers of Carbon Export Efficiency in the Global Ocean.
761 Global Biogeochemical Cycles 33: 891-903.
762 Herraiz-Borreguero, L., D. Lannuzel, P. van der Merwe, A. Treverrow and J. B. Pedro (2016). Large flux of
763 iron from the Amery Ice Shelf marine ice to Pyrdz Bay, East Antarctica. Journal of Geophysical Research:
764 Oceans 121(8): 6009 - 6020.
765 Hoch, M. P. and D. L. Kirchman (1995). Ammonium uptake by heterotrophic bacteria in the Delaware
766 estuary and adjacent coastal waters. Limnology and Oceanography 40(5): 886-897.
767 Karl, D. M., J. R. Christian, J. E. Dore and R. M. Letelier (1996). Microbiological oceanography in the
768 region west of the Antarctic Peninsula: microbial dynamics, nitrogen cycle and carbon flux. Washington,
769 DC, American Geophysical Union.
770 Karnovsky N., D. G. Ainley and P. Lee (2007) Chapter 12 The impact and importance of production in
771 polynyas to top-trophic predators: three case histories. Elsevier Oceanography Series. 74: 391-410
772 Kérouel, R. and A. Aminot (1997). Fluorometric determination of ammonia in sea and estuaring waters by
773 direct segmented flow analysis. Marine Chemistry 57: 265-275.
774 Kim, B., S. H. Lee, S. Y. Ha, J. Jung, T. Kim, E. J. Yang, N. Jo, Y. Lim, J. Park and S. H. Lee (2018).
775 Vertical distribution of macromolecular composition of particulate organic matter in the water column of
776 the Amundsen Sea Polynya during the summer of 2014. Journal of Geophysical Research: Oceans 123:
777 1393 - 1405.
778 Knap, A., A. Michaels, and A. Close. (1994). JGOFS Protocols. JGOFS Plan. Off. Woods Hole, MA, US
779 198.
780 Koike, I., O. Holm-Hansen and D. C. Biggs (1986). Inorganic nitrogen metabolism by Antarctic
781 phytoplankton with special reference to ammonium cycling. Marine Ecology Progr. Series 30: 105-116.
782 Kopczyńska, E. E., N. Savoye, F. Dehairs, D. Cardinal and M. Elskens (2007). Spring phytoplankton
783 assemblages in the Southern Ocean between Australia and Antarctica. Polar Biology 31(1): 77-78.
784 Lannuzel, D., A. R. Bowie, P. C. van der Merwe, A. T. Townsend and V. Schoemann (2011). Distribution
785 of dissolved and particulate metals in Antarctic sea ice. Marine Chemistry 124(1–4): 134-146.
786 Laufkötter, C., M, Vogt, N. Gruber, M. Aita-Noguchi, O. Aumont, L. Bopp, E. Buitenhuis, S.C. Doney, J.
787 Dunne, T. Hashioka, J. Hauck, T. Hirata, J. John, C. Le Quéré, I. D. Lima, H. Nakano, R. Seferian, I.
788 Totterdell, M. Vichi and C. Völker (2015) Drivers of future marine primary production. Biogeosciences
789 12: 6955-6984
790 Laws, E. A. and K. Maiti (2019). The relationship between primary production and export production in the
791 ocean: Effects of time lags and temporal variability. Deep Sea Res. I: Oceanographic Research Papers
792 148: 100-107.

Leblanc K., B. Quéguiner, F. Diaz, V. Cornet, M. Michel-Rodriguez, X. D. de Madron, C. Bowler, S. Malviya, M. Thyssen, G. Grégori, M. Rembauville, O. Grosso, J Poulain, C. de Vargas, M. Pujo-Pay and P. Conan (2018) Nanoplanktonic diatoms are globally overlooked but play a role in spring blooms and carbon export. Nature Communications 9 (953): 1-12

Le Moigne, F. A. C., S. Henson, E. Cavan, C. Georges, K. Pabortsava, E. P. Achterberg, E. Ceballos-Romero, M. V. Zubkov and R. J. Sanders (2016). What causes the inverse relationship between primary production and export efficiency in the Southern Ocean. Geophysical Research Letters 43: 4457-4466.

Lee, S.H, J. Hwang, H.W. Ducklow, D. Hahm, S.H. Lee, D. Kim, J.H. Hyun, J. Park, H. K. Ha, T.W. Kim, E. J. Yang and H. C. Shin (2017). Evidence of minimal carbon sequestration in the productive Amundsen Sea polynya. Geophysical Research Letters 44: 7892-7899

Letscher, R. T., and J. K. Moore (2015). Preferential remineralization of dissolved organic phosphorus and non-Redfield DOM dynamics in the global ocean: Impacts on marine productivity, nitrogen fixation and carbon export. Global Biogeochemical Cycles 29: 325-340

Liénart, C., N. Susperregui, V. Rouaud, J. Cavalheiro, V. David, Y. Del Amo, R. Duran, B. Lauga, M. Monperrus, T. Pigot, S. Bichon, K. Charlier and N. Savoye (2016). Dynamics of particulate organic matter in a coastal system characterized by the occurrence of marine mucilage – A stable isotope study. Journal of Sea Research 116: 12-22.

Lin, H., S. Rauschenberg, C. R. Hexel, T. J. Shaw and B. S. Twining (2011). Free-drifting icebergs as sources of iron to the Weddell Sea. Deep Sea Research Part II: Topical Studies in Oceanography 58(11–12): 1392-1406.

Liniger, G., P. G. Strutton, D. Lannuzel and S. Moreau (2020). Calving event led to changes in phytoplankton bloom phenology in the Mertz Polynya, Antarctica. Journal of Geophysical Research: Oceans, 125, e2020JC016387.

Maiti, K., M. Charette, K. O. Buesseler and M. Kahru (2013). An inverse relationship between production and export efficiency in the Southern Ocean. Geophys. Res. Lett. 40: 1557-1561.

Marinov, I., A. Gnanadesikan, J. R. Toggweiler and J. L. Sarmiento (2006). The Southern Ocean biogeochemical divide. Nature 441(7096): 964-967.

Martin, J. (1990). Glacial-interglacial CO_2 change: The Iron Hypothesis. Paleoceanography 5(1): 1-13.

McGillicuddy, D. J., P. N. Sedwick, M. S. Dinniman, K. R. Arrigo, T. S. Bibby, B. J. W. Greenan, E. E. Hofmann, J. M. Klinck, W. O. Smith Jr, S. L. Mack, C. M. Marsay, B. M. Sohst and G. L. van Dijken (2015). Iron supply and demand in an Antarctic shelf ecosystem. Journal of Geophysical Research 42(19): 8088-8097.

825 Mengesha, S., F. Dehairs, M. Fiala, M. Elskens and L. Goeyens (1998). Seasonal variation of phytoplankton
826 community structure and nitrogen uptake regime in the Indian Sector of the Southern Ocean. Polar
827 Biology 20(4): 259-272.
828 Mishonov, A. V., W. D. Gardner and M. J. Richardson (2003). Remote sensing and surface POC
829 concentration in the South Atlantic. Deep Sea Research II 50: 2997-3015.
830 Montes-Hugo M., Doney S.C, Ducklow H.W., Fraser W., Martinson D., Stammerjohn S.E., and O. Schofield
831 (2009) Recent changes in phytoplankton communities associated with rapid regional climate change along
832 the Western Antarctic Peninsula. Science 232(5920): 1470-1473
833 Moreau, S., L. D., J. J, M. Arroyo, M. Corkill, E. Cougnon, C. Genovese, B. Legresy, A. Lenton, V.
834 Puigcorbé, L. Ratnarajah, S. R. Rintoul, M. Roca-Martí, M. Rosenberg, E. H. Shadwick, A. Silvano, P.
835 G. Strutton and B. Tilbrook (2019). Sea Ice Meltwater and Circumpolar Deep Water Drive Contrasting
836 Productivity in Three Antarctic Polynyas. Journal of Geophysical Research: Oceans 124(5): 2943-2968.
837 Moreau, S., Boyd, P.W. and Strutton, P.G. (2020). Remote assessment of the fate of phytoplankton in the
838 Southern Ocean sea-ice zone. Nature Communications 11**,** 3108.
839 Moreau, S., E. di Fiori, I. R. Schloss, G. O. Almandoz, J. L. Esteves, F. E. Paparazzo, G. A. Ferreyra (2013).
840 Deep-Sea Research Part I: Oceanographic Research Papers, 82, 44:59.
841 Obernosterer I, M. Fourquez and S. Blain S (2015). Fe and C co-limitation of heterotrophic bacteria in the
842 naturally fertilized region off the Kerguelen Islands. Biogeosciences 12 (6): 1983-1992
843 Owens, N. P. J., J. Priddle and M. J. Whitehouse (1991). Variations in phytoplanktonic nitrogen assimilation
844 around South Georgia and the Bransfield Strait (Southern Ocean). Marine Chemistry 35: 287-304.
845 Owens, S. A., K. O. Buesseler and K. W. W. Sims (2011). Re-evaluating the ^{238}U-salinity relationship in
846 seawater: Implications for the ^{238}U-^{234}Th disequilibrium method. Marine Chemistry 127: 31-39.
847 Pasquer, B., M. Mongin, N. Johnston and S. Wright (2010). Distribution of particulate organic matter (POM)
848 in the Southern Ocean during BROKE-West (30°E - 80°E). Deep Sea Research II: Topical Studies in
849 Oceanography 57(9-10): 779-793.
850 Passow, U., A. L. Alldredge and B. E. Logan (1994). The role of particulate carbohydrate exudates in the
851 flocculation of diatom blooms. Deep Sea Res. I: Oceanographic Research Papers 41: 335-357.
852 Passow, U. and C. A. Carlson (2012). The biological pump in a high CO2 world. Marine Ecology Progress
853 Series 470: 249-271.
854 Puigcorbé V., M Roca-Martí, P. Masque, C. R. Benitez-Nelson, M. Rutgers v. d. Loeff, L. M. Laglera, A.
855 Bracher, W. Cheah, V. H. Strass, M. Hoppema, J. Santos-Echeandia, B. P, V. Hunt, E. A. Pakhomov and
856 C. Klaas (2017a): Particulate organic carbon export across the Antarctic Circumpolar Current at 10°E:
857 Differences between north and south of the Antarctic Polar Front. Deep Sea Research Part II: Topical
858 Studies in Oceanography, 138, 86-101.

Puigcorbé V., M Roca-Martí, P. Masque, C. R. Benitez-Nelson, M. Rutgers v. d. Loeff, L. A. Bracher and S. Moreau (2017b). Latitudinal distributions of particulate carbon export across the North Western Atlantic Ocean. Deep-Sea Research Part I: Oceanographic Research Papers, 129, 116:130.

Puigcorbé V., P. Masqué and F.A. C. Le Moigne (2020). Global database of ratios of particulate organic carbon to thorium-234 in the ocean: improving estimates of the biological carbon pump. Earth Systems Science Data, 12: 1267-1285.

R Core Team (2014). R: A language and environment for statistical computing. R Foundation for Statistical Computing, Vienna, Austria. ISBN 3-900051-07-0, URL http://www.R-project.org/.

Ratnarajah, L., S. Nicol and A. R. Bowie (2018). Pelagic iron recycling in the Southern Ocean: Exploring the contribution of marine animals. Frontiers in Marine Science 5(109):

Roca-Martí, M., V. Puigcorbé, M. H. Iversen, M. Rutgers van der Loeff, C. Klaas, W. Cheah, A. Bracher and P. Masqué (2017). High particulate organic carbon export during the decline of a vast diatom bloom in the Atlantic sector of the Southern Ocean. Deep Sea Research II: Topical Studies in Oceanography 138: 102-115.

Romero, O. and L. K. Armand (2010). Marine diatoms as indicators of modern changes in oceanographic conditions. Cambridge University Press

Rosenberg M and Rintoul S (2017). Aurora Australis Marine Science Cruise AU1602, Dalton, Mertz and Ninnis CTDs - Oceanographic Field Measurements and Analysis (https://researchdata.ands.org.au/aurora-australis-marine-measurements-analysis/1358680?fl)

Sedwick, P. N., A. R. Bowie and T. W. Trull (2008). Dissolved iron in the Australian sector of the Southern Ocean (CLIVAR SR3 section): Meridional and seasonal trends. Deep Sea Research Part I: Oceanographic Research Papers 55(8): 911-925.

Sedwick, P. N. and G. R. Di Tullio (1997). Regulation of algal blooms in Antarctic shelf waters by the release of iron from melting sea ice. Geophysical Research Letters 24: 2515-2518.

Smetacek, V., C. Klaas, V. H. Strass, P. Assmy, M. Montresor, B. Cisewski, N. Savoye, D. J. Webb, F. d'Ovidio, J. M. Arrieta, U. Bathmann, R. Bellerby, G. M. Berg, P. Croot, S. Gonzalez, J. Henjes, G. J. Herndl, L. J. Hoffmann, H. Leach, M. Losch, M. M. Mills, C. Neill, I. Peeken, R. Röttgers, O. Sachs, E. Sauter, M. M. Schmidt, J. Schwarz, A. Terbrüggen and D. A. Wolf-Gladrow (2012). Deep carbon export from a Southern Ocean iron-fertilized diatom bloom. Nature 487(313): 1-26.

Smith Jr. W. O, C.A. Carlson, H. W. Ducklow and D. A. Hansell (1998). Growth dynamics of *Phaeocystis antarctica*- dominated plankton assemblages from the Ross Sea. Marine Ecology Progress Series. 168: 229-244

Stange P., L. T. Bach, F. A. C Le Moigne, J. Taucher, T. Boxhammer and U. Riebesell (2017) Quantifying the time lag between organic matter production and export in the surface ocean: Implications for estimates of export efficiency. Geophysical Research Letters. 44 (1): 268-276

Steinberg, D. K. and M. R. Landry (2017). Zooplankton and the Ocean Carbon Cycle. Annual Review of Marine Science 9: 413-444.

Sterner, R. W., and J. J. Elser (2002). Ecological stoichiometry: The biology of elements from molecules to the biosphere, 1st ed. Princeton Univ. Press.

Thomson, R. E. and I. V. Fine (2003). Estimating mixed layer depth from oceanic profile data. Journal of Atmospheric and Oceanic Technology. 20: 319-329.

Tréguer, P., C. Bowler, B. Moriceau, S. Dutkiewicz, M. Gehlen, O. Aumont, L. Bittner, R. Dugdale, Z. Finkel, D. Ludicone, O. Jahn, L. Guidi, M. Lasbleiz, K. Leblanc, M. Levy and P. Pondaven (2017). Influence of diatom diversity on the ocean biological carbon pump. Nature Geosc. 11: 27–37.

Turley C. M., and P. J. Mackie (1994). Biogeochemical significance of attached and free-living bacteria and the flux of particles in the NE Atlantic Ocean. Marine Ecology Progress Series. 115: 191-203

Turner, J. T. (2015). Zooplankton fecal pellets, marine snow, phytodetritus and the ocean's biological pump. Progress in Oceanography 130(0): 205-248.

Yager P.L., R.M. Sherrell, S.E. Stammerjohn, H.W. Ducklow, O.M.E. Schofield, E.D. Ingall, S.E. Wilson, K.E. Lowry, C.M. Williams, L. Riemann, S. Bertilsson, A.C. Alderkamp, J. Dinasquet, R. Logares, I. Richert, R.E. Sipler, A.J. Melara, L. Mu, R.G. Newstead, A.F. Post, R. Swalethorp and G.L. van Dijken (2016). A carbon budget for the Amundsen Sea Polynya, Antarctica: Estimating net community production and export in a highly productive polar ecosystem. Elementa: Science of the Anthropocene 1-37

Figures and Tables

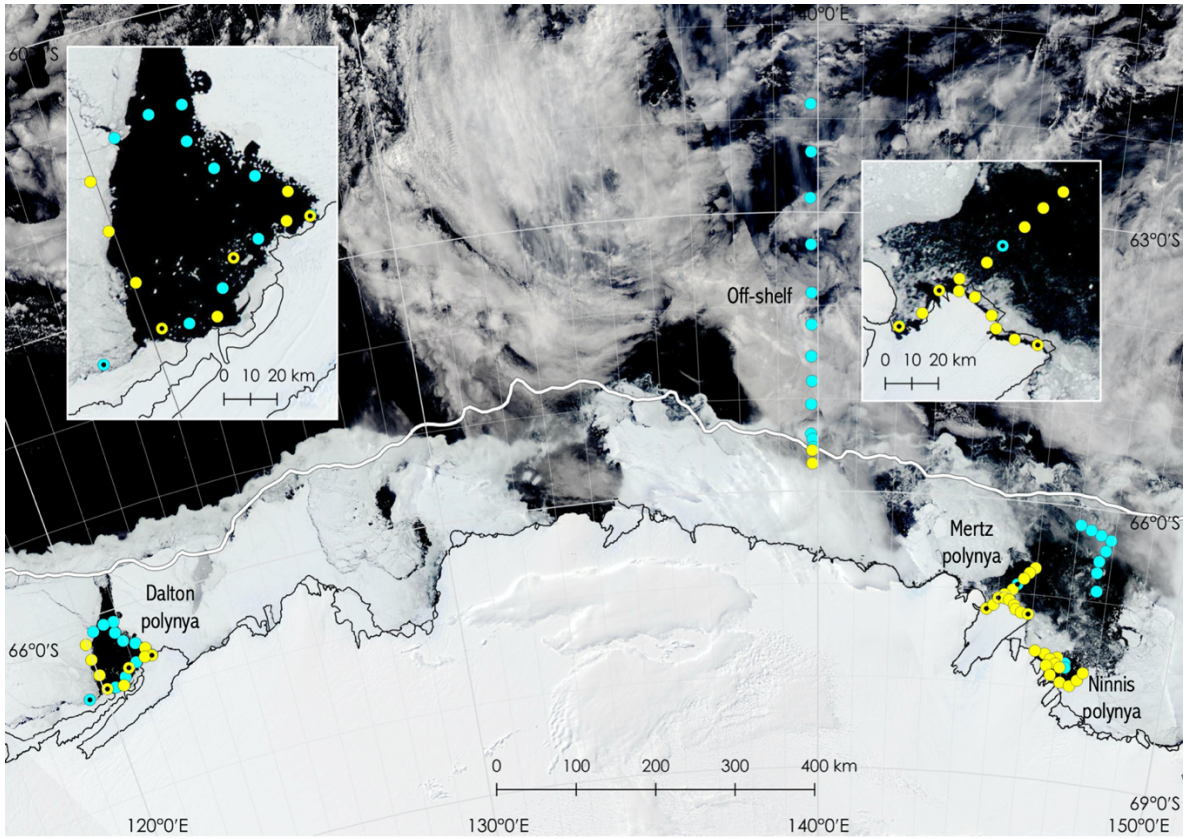

Figure 1: Station location for the Dalton, Mertz and Ninnis polynyas, and the off-shelf region. Yellow dots denote sites where discrete particulate organic carbon measurements were taken. Blue dots represent sites where particulate organic carbon was extrapolated based on measurements of particulate beam attenuation coefficient at 660 nm. Smaller black dots represent where thorium-234 samples were taken. The thick white line indicates the shelf break. Background image from NASA Worldview (https://worldview.earthdata.nasa.gov).

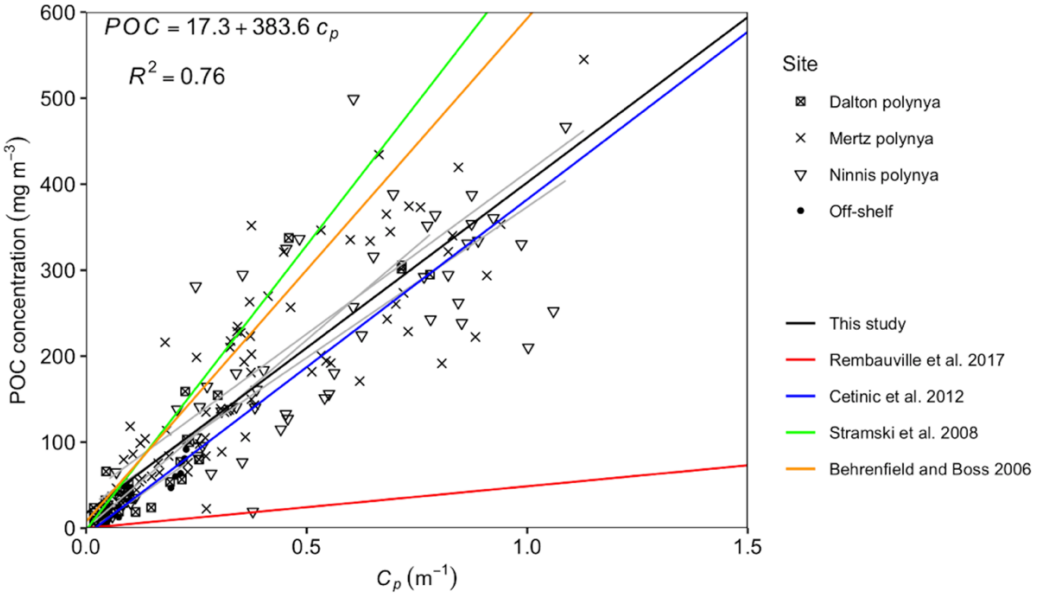

Figure 2: Relationship between in situ particulate organic carbon (POC) concentration (mg m^{-3}) and particulate beam attenuation coefficient (c_p, m^{-1}). Grey lines indicate the slope for each site. We found no evidence of site differences (p = 0.1); therefore, one common line (black line) fits all sites. Overlaid are the relationships reported by previous studies for comparison.

Table 1: Mixed layer depth, euphotic depth, particulate organic carbon (POC) concentration and integrated POC at various depths for the Dalton, Mertz and Ninnis polynyas, and the off-shelf sites. Values presented are mean ± standard deviation and median values in brackets.

Parameter	Dalton polynya	Mertz polynya	Ninnis polynya	Off-shelf sites
Mixed layer depth (m)	43 ± 43 (28)	13 ± 1 (12)	13 ± 2 (12)	20 ± 7 (17)
Euphotic depth (m)	95 ± 56 (97)	40 ± 9 (40)	41 ± 6 (40)	113 ± 45 (118)
POC Within euphotic zone (mg m^{-3})	59 ± 58 (34)	244 ± 71 (246)	275 ± 95 (284)	58 ± 27 (56)
POC Top 200 m (mg m^{-3})	60 ± 62 (32)	121 ± 95 (82)	138 ± 124 (77)	47 ± 26 (34)
Integrated POC Top 200 m (g m^{-2})	12 ± 7 (8)	23 ± 6 (23)	27 ± 6 (28)	9 ± 1 (9)
Integrated POC 200 – 500 m (g m^{-2})	4 ± 3 (3)	7 ± 3 (8)	8 ± 1 (8)	6 ± 2 (7)

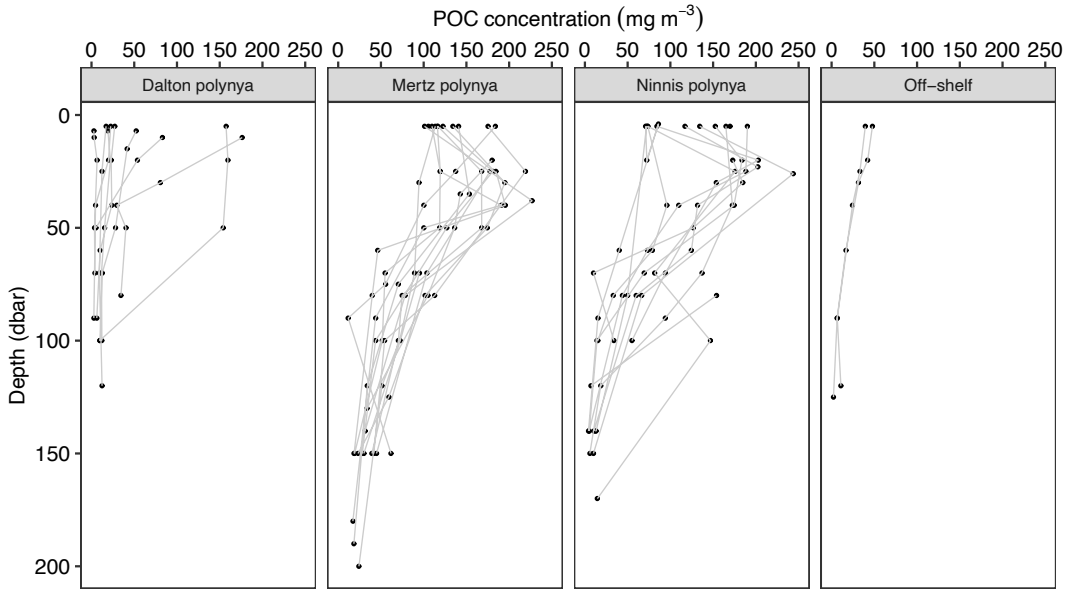

933
934
935 **Figure 3:** Particulate organic carbon (POC) concentrations (mg m^{-3}) based on *in situ* measurements in the
936 Dalton, Mertz, and Ninnis polynyas, and at the off-shelf stations.
937

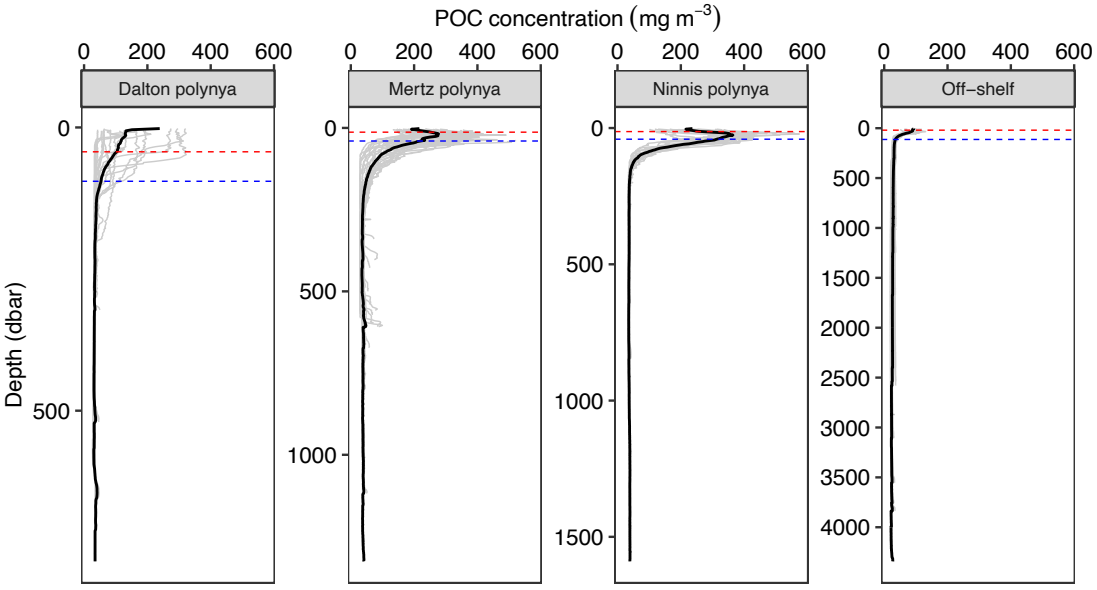

938
939
940 **Figure 4:** Particulate organic carbon (POC) profiles extrapolated based on the linear regression between
941 POC and c_p (Fig. 3) across the entire water column for the Dalton, Mertz, and Ninnis polynyas, and the off-
942 shelf sites. Grey lines represent individual station profiles, and the black line represents the mean profile.
943 Note the varying scales for depth on the y-axis. Red dashed horizontal line represents average mixed layer
944 depth, whilst the blue dashed horizontal line represents the average euphotic depth.

945 **a)**

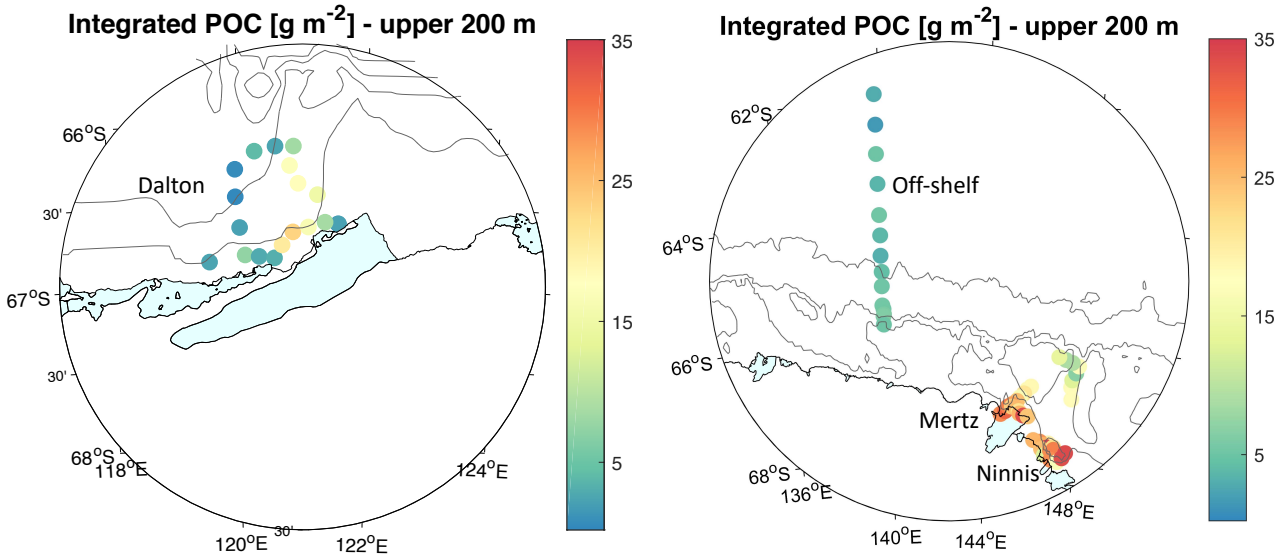

946

947 **b)**

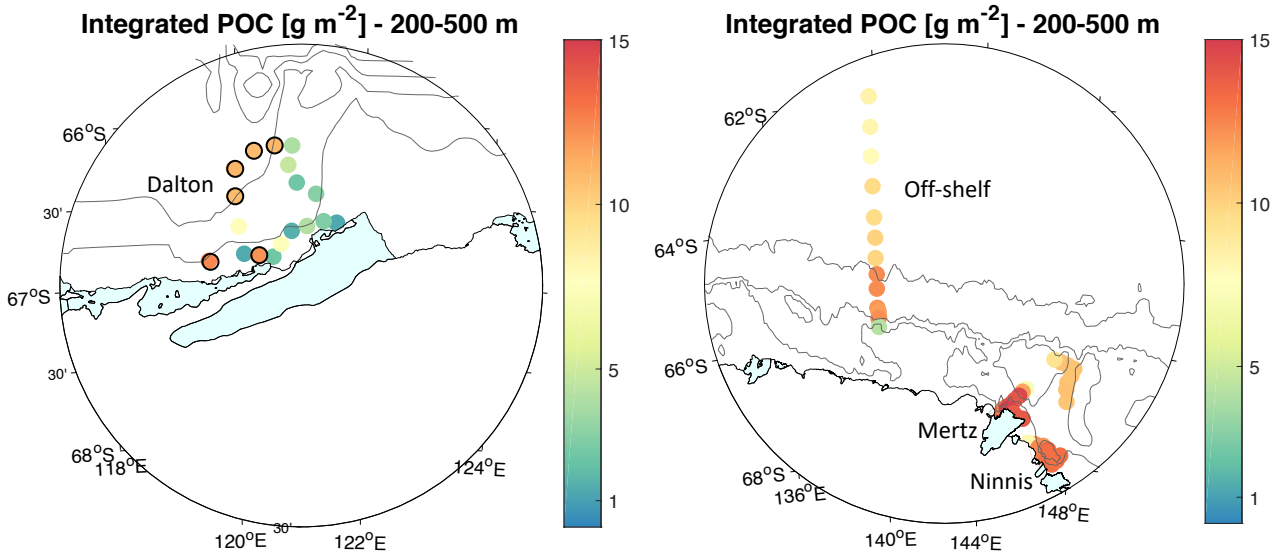

948

949 **Figure 5:** Depth integrated particulate organic carbon (POC, g m^{-2}) in (a) the top 200 m, and (b) between
950 200 and 500 m (or bottom depth), for the Dalton, Mertz, and Ninnis polynyas, and the off-shelf sites. The
951 black circles at the Dalton polynya denote those stations that reached 500 m (n = 6) the others (n = 13; the
952 dot found in the most southeast location represents two stations) had depths between 230 and 322 m. Note
953 the varying scales for POC stocks.

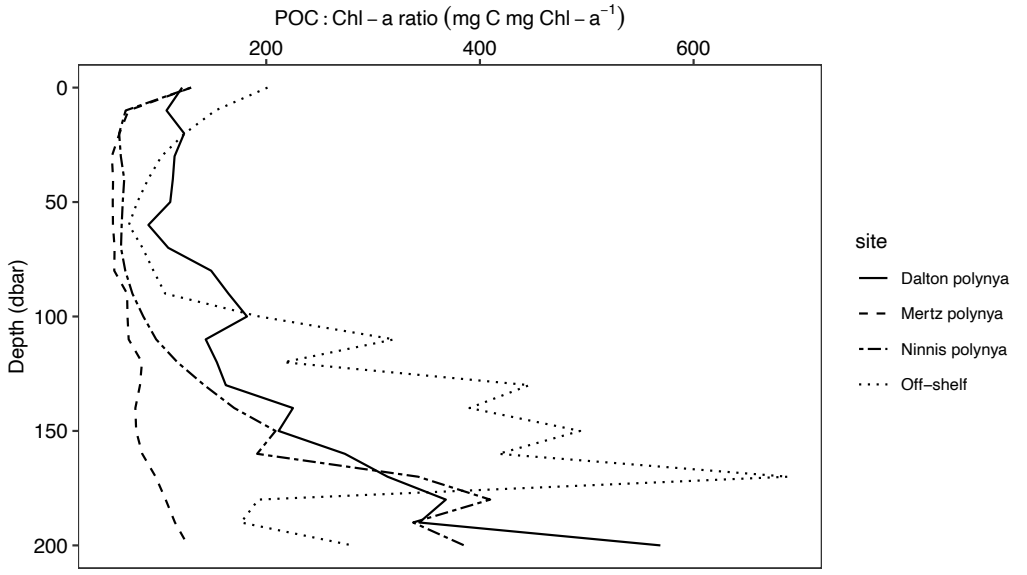

Figure 6: Mean ratio of particulate organic carbon (POC) to chlorophyll-a (Chl-a) in the polynyas and off-shelf sites averaged every 10 dbar.

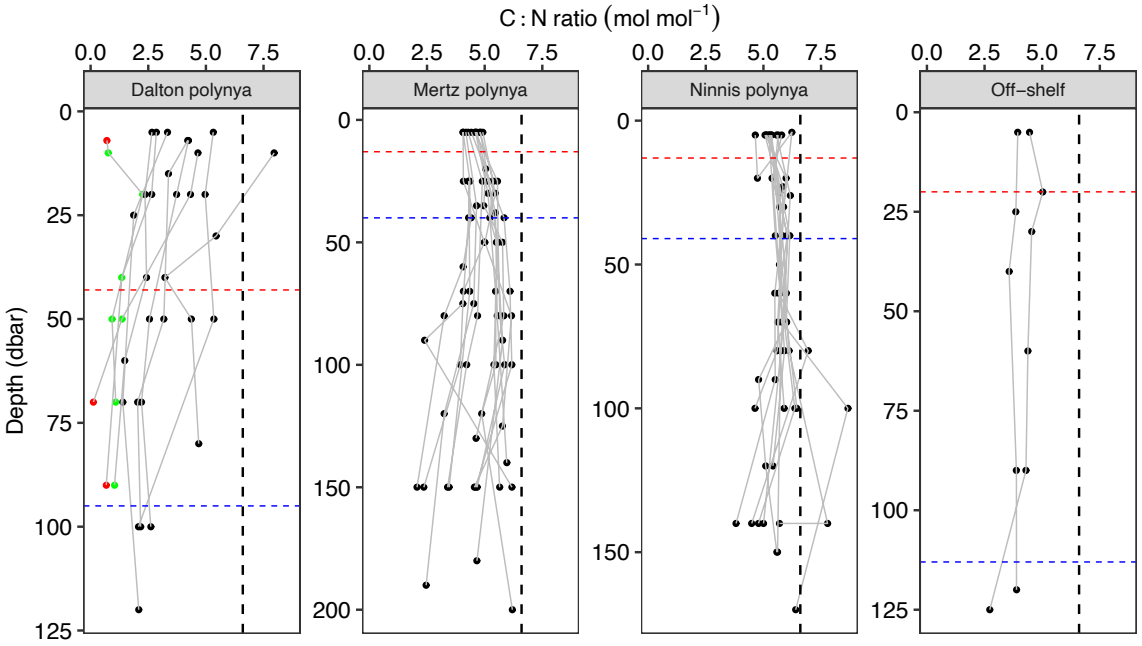

Figure 7: Particulate organic carbon:nitrogen (C:N) ratios (mol mol^{-1}) in the Dalton, Mertz, and Ninnis polynyas, and at the off-shelf sites. In the Dalton polynya, the green points show samples where the blank contributed 31 – 46 % to C (n = 7), whilst the red points show samples where the blank contributed 50 – 52 % (n = 3), and thus need to be taken with caution. Black dashed vertical line indicates the Redfield ratio (6.6). The blue and red dashed horizontal lines represent the average euphotic depth and the average mixed layer depth, respectively.

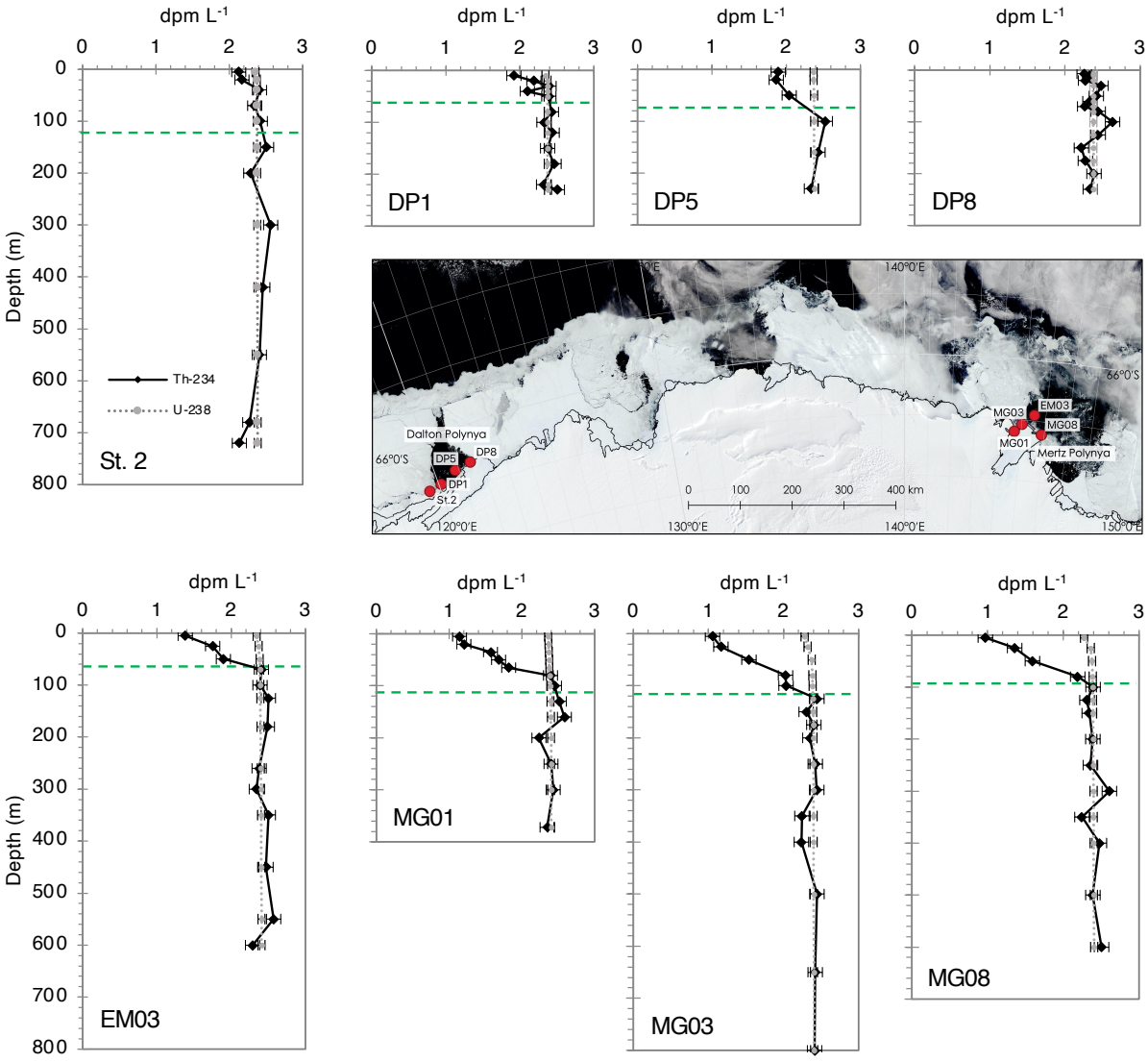

Figure 8: Thorium-234 (^{234}Th, black diamonds) and uranium-238 (^{238}U, grey dotted line) concentration profiles along the water column at each station. The top four panels are stations located in the Dalton polynya and the lower four panels are stations sampled within the Mertz polynya. The green horizontal dashed lines show the depths at which fluorescence was 10% of its maximum signal in overlying waters (primary production zone, PPZ). The fluorescence profile was not available for station DP8. The map in the centre shows the location of the stations sampled in each polynya.

Table 2: Thorium-234 (^{234}Th) fluxes estimated at several depth horizons: shallow *in situ* pump (ISP) depth, equilibrium depth (Eq depth), primary production zone (PPZ) and euphotic zone depth (Zeu). See section 2.2 for details. Particulate organic carbon fluxes are also provided, at the depth of the shallow ISP and at 300 m.

Polynya	Station	Shallow ISP depth (m)	^{234}Th flux at shallow ISP depth (dpm m^{-2} d^{-1})	Eq depth (m)	^{234}Th flux at Eq depth (dpm m^{-2} d^{-1})	PPZ depth (m)	^{234}Th flux at PPZ depth (dpm m^{-2} d^{-1})	Zeu depth (m)	^{234}Th flux at Zeu (dpm m^{-2} d^{-1})	POC fluxes at shallow ISP depth (mmolC m^{-2} d^{-1})
Dalton	2	100	167 ± 189	40	175 ± 91	40	175 ± 91	122	112 ± 214	1.2 ± 1.3
	DP1	100	279 ± 168	30	234 ± 73	58	299 ± 103	74	284 ± 128	3.0 ± 1.8
	DP5	160	600 ± 332	100	774 ± 236	68	689 ± 161	20	280 ± 75	6.0 ± 3.3
	DP8	150	-125 ± 205	surface	-	ND	-	170	-48 ± 225	-
Mertz	EM03	100	1122 ± 179	70	1127 ± 135	60	1059 ± 115	26	609 ± 56	9.3 ± 1.5
	MG01	100	1805 ± 183	80	1824 ± 131	108	1784 ± 190	44	1306 ± 72	16.3 ± 1.7
	MG03	100	2297 ± 206	125	2405 ± 228	114	2357 ± 216	46	1462 ± 96	24.7 ± 2.2
	MG08	100	1977 ± 193	100	1977 ± 193	86	1938 ± 155	54	1552 ± 99	15.0 ± 1.5

ND = No data

Table 2: Thorium-234 (^{234}Th) fluxes estimated at several depth horizons: shallow *in situ* pump (ISP) depth, equilibrium depth (Eq depth), primary production zone (PPZ) and euphotic zone depth (Zeu). See section 2.2 for details. Particulate organic carbon fluxes are also provided, at the depth of the shallow ISP and at 300 m.

Polynya	Station	Shallow ISP depth (m)	^{234}Th flux at shallow ISP depth (dpm m^{-2} d^{-1})	Eq depth (m)	^{234}Th flux at Eq depth (dpm m^{-2} d^{-1})	PPZ depth (m)	^{234}Th flux at PPZ depth (dpm m^{-2} d^{-1})	Zeu depth (m)	^{234}Th flux at Zeu (dpm m^{-2} d^{-1})	POC fluxes at shallow ISP depth (mmolC m^{-2} d^{-1})
Dalton	2	100	167 ± 189	40	175 ± 91	40	175 ± 91	122	112 ± 214	1.2 ± 1.3
	DP1	100	279 ± 168	30	234 ± 73	58	299 ± 103	74	284 ± 128	3.0 ± 1.8
	DP5	160	600 ± 332	100	774 ± 236	68	689 ± 161	20	280 ± 75	6.0 ± 3.3
	DP8	150	-125 ± 205	surface	-	ND	-	170	-48 ± 225	-
Mertz	EM03	100	1122 ± 179	70	1127 ± 135	60	1059 ± 115	26	609 ± 56	9.3 ± 1.5
	MG01	100	1805 ± 183	80	1824 ± 131	108	1784 ± 190	44	1306 ± 72	16.3 ± 1.7
	MG03	100	2297 ± 206	125	2405 ± 228	114	2357 ± 216	46	1462 ± 96	24.7 ± 2.2
	MG08	100	1977 ± 193	100	1977 ± 193	86	1938 ± 155	54	1552 ± 99	15.0 ± 1.5

ND = No data

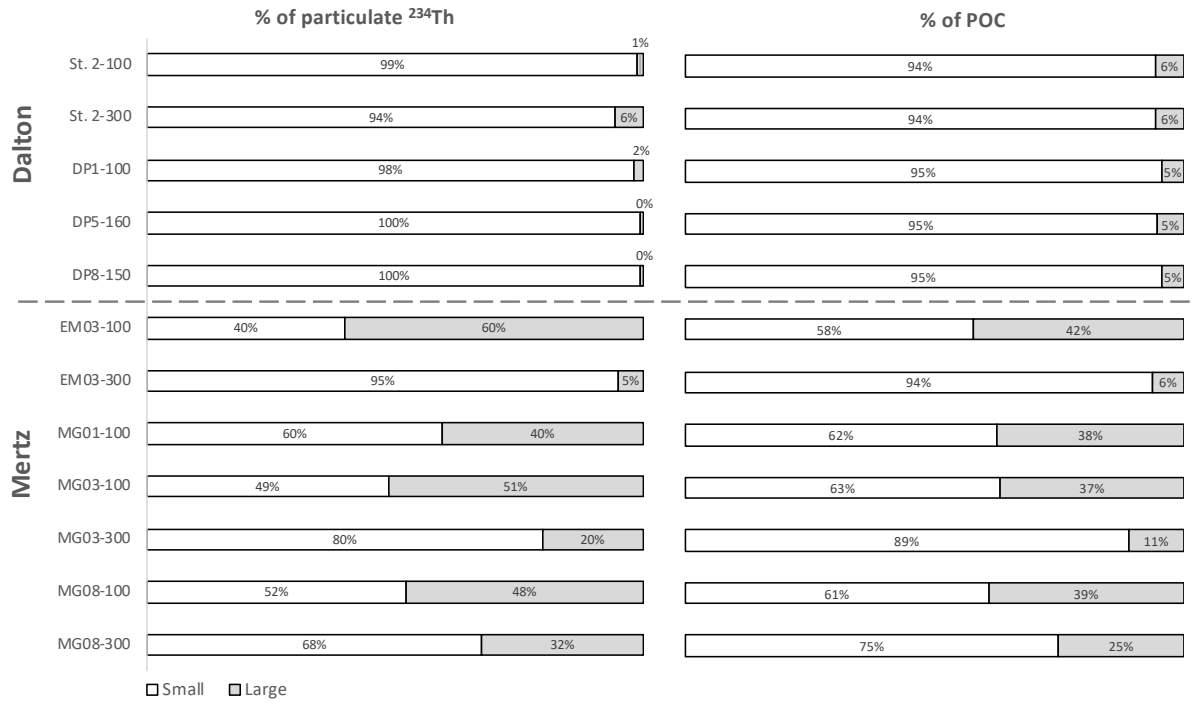

Figure 9: Particulate thorium-234 (^{234}Th) and particulate organic carbon (POC) fractionation between small (1-53 µm) and large (> 53 µm) particles at different stations and depths in the Dalton and Mertz polynyas. Note that the number next to the station name refers to the sampling depth (e.g., St.2-100 refers to samples collected at St.2 at 100 m depth).

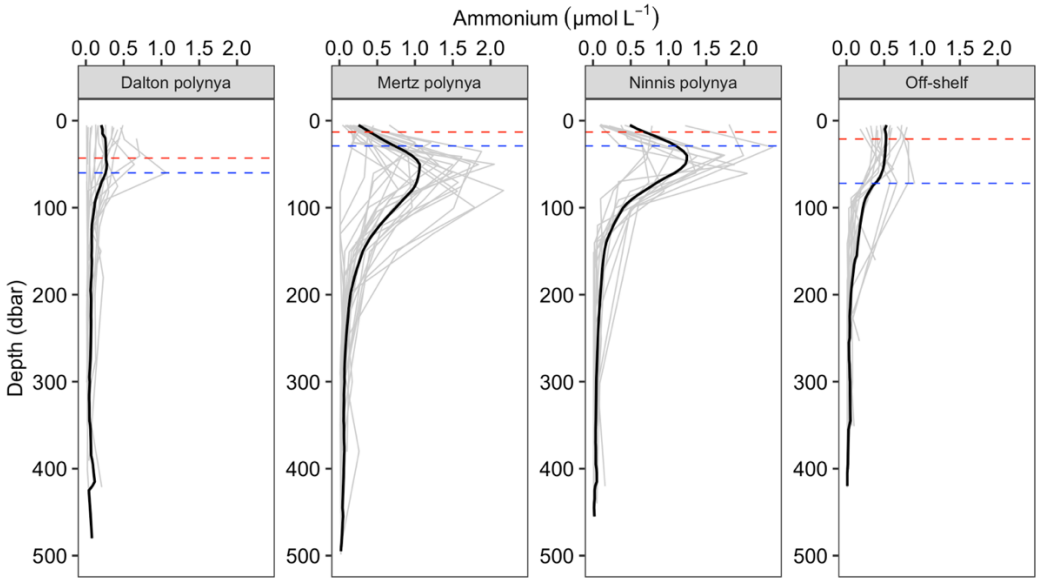

Figure 10: Concentration of ammonium (µmol L^{-1}) in the Dalton, Mertz, and Ninnis polynyas, and at the off-shelf sites. Grey lines represent ammonia concentrations as measured from the CTD bottle samples. Solid black line indicates mean ammonium concentration across all stations and averaged every 5 dbar. Blue dashed horizontal line represents the average euphotic depth. Red dashed horizontal line represents the average mixed layer depth.